

# Integration of domestic ventilation systems with vertical axis wind turbine ventilation technology

Jirayut Sitthipuk

A thesis submitted in partial fulfilment of the requirement of Edinburgh Napier University, for the award of Master of Research

March 2022

## Abstract

The integration of natural ventilation components has become increasingly desirable in the building sector as a means to enhance ventilation systems. Low carbon technologies, such as windcatchers and turbine ventilators, are commonly employed in commercial, educational, and industrial buildings for cooling and ventilation purpose. This study investigates a novel concept of home ventilation systems integrated with a vertical axis wind turbine, aiming to provide a detailed understanding of the system's ventilation performance concerning both air extraction and supply using a turbine ventilator.

Performing Computational Fluid Dynamics (CFD) simulations, the 8-blade turbine ventilator achieved a maximum exhaust flow rate of 87.52 l/s at a wind speed of 6 m/s, exceeding the minimum ventilation rate. Additionally, the initial design of the air intake vent (AIV) was tested, resulting in a maximum air supply flow rate of 38.25 l/s at 6 m/s. Subsequent modifications to the AIV were made, yielding two variants: AIV1 and AIV2, which improved ventilation performance by 5% and 20% respectively.

Given that the proposed turbine ventilator is in its initial design phase, the numerical results demonstrate promising potential of the development of a home ventilation system integrated with the turbine ventilator. This study serves as a foundation for further research and optimisation of such systems.

## Acknowledgements

I would like to express my heartfelt gratitude and appreciation to my esteemed supervisors, Professor John Currie, and Dr Julio Bros-Williamson for their unwavering support, invaluable guidance, and constructive feedback throughout my research journey.

I would also like to extend my deepest appreciation to my family for their unwavering love, patience, and support throughout this challenging yet rewarding journey. Their faith in my abilities and constant encouragement have been the bedrock of my success.

# Table of Contents

- ABSTRACT..... I
  
- ACKNOWLEDGEMENTS ..... II
  
- LIST OF TABLE..... II
  
- LIST OF FIGURE ..... III
  
- LIST OF ABBREVIATIONS..... VII
  
- LIST OF SYMBOL..... IX
  
- 1. INTRODUCTION..... 1
  - 1.1. Background .....1
  - 1.2. Research Questions.....7
  - 1.3. Research Objectives .....7
  - 1.4. Scope .....8
  
- 2. LITERATURE REVIEW ..... 10
  - 2.1. Influence of Ventilation Systems on Domestic Dwellings.....10
  - 2.2. Applications of Ventilation Technology for Energy Efficiency .....11

2.3.	Natural Ventilation Systems in Building.....	13
2.4.	Wind-Driven Ventilation Technologies for Domestic Dwellings.....	14
2.5.	Vertical Axis Wind Technology as Active Wind Driven Ventilation .....	16
2.6.	Potential of Turbine Ventilator in Domestic Ventilation System.....	17
2.7.	Application of Computational Fluid Dynamics Approach .....	18
3.	<b>METHODOLOGY .....</b>	<b>21</b>
3.1.	Modelling Turbine Ventilator.....	23
3.2.	Turbulence Modelling.....	28
3.3.	Computational Domain.....	33
3.4.	Boundary Conditions.....	37
3.5.	Mesh Generation .....	39
4.	<b>RESULTS AND DISCUSSION.....</b>	<b>44</b>
4.1.	The Initial Turbine Ventilator Model.....	44
4.1.1.	Air Extraction Performance.....	46
4.1.1.1.	2-Blade Turbine Ventilator (2B-TV) .....	46
4.1.1.2.	8-Blade Turbine Ventilator (8B-TV) .....	51
4.1.2.	Air intake vent (AIV).....	55

4.1.3.	Performance Comparison and Analysis of Proposed Turbine Ventilator Design.....	58
4.2.	Modifications of Turbine Ventilator Model .....	62
4.2.1.	Blade Height Reduction .....	63
4.2.2.	Modifications of Design Features of Air Intake Vent.....	69
5.	CONCLUSIONS.....	76
5.1.	Research Limitations .....	78
6.	FUTURE WORKS .....	80
	APPENDIX TABLES .....	88
	APPENDIX FIGURES .....	91

## List of Table

Table 3.1. Commercial turbine ventilation technologies (Ventilationland, 2021).....	24
Table 3.2. Rotational speeds for CFD simulation.....	39
Table 4.1. CFD simulation results of ventilation performance for 2B-TV model.....	50
Table 4.2. CFD simulation results of ventilation performance for 8B-TV model.....	55
Table A1. Minimum ventilation rate (air extraction).....	88
Table A2. Minimum ventilation rate (fresh air supply).....	88
Table A3. Ventilation rate of the air intake vent.....	89
Table A4. SimScale' supply flow rate of modified AIV1.....	89
Table A5. SimScale' supply flow rate of modified AIV2.....	89
Table A6. Autodesk's exhaust flow rate of modified 10B-TV.....	90
Table A7. Autodesk's supply flow rate of modified AIV1.....	90

# List of Figure

Figure 1.1. Schematic of concept of home ventilation system.....	4
Figure 1.2. Wind-powered turbine Savonius (a) and Wind-powered fan VT turbine (b) (Ventilationland, 2021). .....	5
Figure 2.1. Schematic diagram of physical experiment setup (Khan et al., 2008a). .....	21
Figure 2.2. Computational domain for CFD simulation (Jadhav et al., 2016).....	21
Figure 3.1. Flowchart of method for application of CFD simulation. ....	23
Figure 3.2. Turbine ventilator model: (a) turbine air extractor and (b) fresh air intake vent. .....	26
Figure 3.3. Schematic: (a) principle of the proposed turbine ventilator, (b) the geometrical parameters of the rotor domain and (c) air intake vent. ....	27
Figure 3.4. CFD computational doamin setup.....	34
Figure 3.5. Comparison of the computational domain optimisation between different sizes. .....	35
Figure 3.6. Modelling of computational domain.....	37
Figure 3.7. Boundary conditions .....	38
Figure 3.8. Mesh details: (a) flow domain, (b) turbine ventilator and (c) inflation layer. ....	41
Figure 3.9. Comparison of velocity magnitudes with different mesh sizes. ....	42



Figure 3.10. Convegence plot of the 8 blade turbine ventilator at velocity = 4 m/s. ....	43
Figure 4.1. CFD simulation setup on SimScale.....	45
Figure 4.2 Velocity contours of initial CFD simulation results in: (a) x-y axis and (b) x-z axis. ....	46
Figure 4.3. Velocity contour of the 2 blade model at different velocities. ....	47
Figure 4.4. Static pressure contours of the 2-blade model at different velocity magnitudes. .....	48
Figure 4.5. Inlet velocity of 4 m/s: (a) velocity vector and (b) pressure contour (at 100 mm above the rotor base). ....	49
Figure 4.6. Inlet velocity of 4 m/s: (a) velocity vector and (b) pressure contour (at 160 mm above the rotor base). ....	50
Figure 4.7. Velocity contours of the 8B-TV model at 100mm above the rotor base.....	51
Figure 4.8. Contours and vector of velocity for the 8B-TV model at velocity of 4 m/s: (a) at 160mm and (b) at 300 mm above the cylindrical base. ....	52
Figure 4.9. Contours of pressure for the 8B-TV model at velocity of 4 m/s: (a) at 160mm and (b) at 300 mm above the cylindrical base.....	53
Figure 4.10. Contours of velocity for the 8B-TV model at 160 mm above the rotor base. ...	54
Figure 4.11. Static pressure constours of the 8B-TV model at 100mm above the rotor base.....	54

Figure 4.12. Contours of velocity for air intake vent at velocity of 6 m/s: (a) at 50 mm, (b) at 100 mm and (c) at 150 mm.....	56
Figure 4.13. Distribution of wind velocity at the bottom of the AIV supply channel: (a) velocity contour and (b) velocity vector. ....	56
Figure 4.14. Contours of pressure for air intake vent at velocity of 6 m/s: (a) at 50 mm, (b) at 100 mm and (c) at 150 mm.....	57
Figure 4.15. Cross-sectional plane of the AIV model at velocity of 6 m/s: (a) velocity and (b) pressure contour. ....	58
Figure 4.16. Comparison of the ventilation performance of 2B-TV and 8B-TV.....	59
Figure 4.17. Comparison of the ventilation performance of the turbine ventilators with other studies. ....	60
Figure 4.18. Volume flow rates induced by the AIV model. ....	61
Figure 4.19. Performance curve of the 8B-TV model.....	62
Figure 4.20. Performance curve of the AIV model. ....	62
Figure 4.21. The modified turbine blades (a) schematic view and (b) 3D CAD model. ....	64
Figure 4.22. Contours of velocity of the modified 10B-TV at various wind speed. ....	65
Figure 4.23. Contours of pressure of the modified 10B-TV at various wind speed.....	66
Figure 4.24. Ventilation performance of modified 10B-TV at a velocity of 6m/s: (a) Velocity vector and (b) pressure contours.....	67

Figure 4.25. Comparison of the modified 10B-TV ventilation performance with the 8B-TV model.....	68
Figure 4.26. Comparison of the modified 10B-TV ventilation performance with other studies. ....	68
Figure 4.27. Schematic of (a) Modified AIV1 and (b) Modified AIV2. ....	69
Figure 4.28. Contours of (a) velocity and (b) pressure of the modified AIV1 at velocity of 6 m/s. ....	70
Figure 4.29. Contours of (a) velocity and (b) pressure of the modified AIV2 at velocity of 6 m/s. ....	71
Figure 4.30. Cross-sectional plane of modified AIV1: (a) velocity contour and (b) pressure contour.....	73
Figure 4.31. Comparison of ventilation performance of the modified AIV1 and the modified 10B-TV. ....	74
Figure A1. Domain maximum error percentage. ....	91
Figure A2. Velocity vector of the modified AIV1 for visualizing flow behaviour in the chamber.....	92
Figure A3. Velocity vector of the modified AIV1 for visualizing flow behaviour within the mode.....	93
Figure A4: The position of result extraction for the air supply rate. ....	93

## List of Abbreviations

2B-TV	2 blade turbine ventilator
8B-TV	8 blade turbine ventilator
10B-TV	10 blade turbine ventilator
AIV	Air intake vent
CAD	Computer-aided design
CFD	Computational Fluid Dynamics
COVID	Coronavirus disease
EU	European Union
HVAC	Heating, ventilation and air-conditioning
IAQ	Indoor air quality
MFR	Multiple frame reference
NZEB	Nearly zero energy building
RANS	Reynolds-Averaged Navier-Stokes
RPM	Revolutions per minute
TV	Turbine ventilator

UK United Kingdom

VHR Ventilation with heat recovery

## List of Symbol

$G_b$	Generation of the turbulent kinetic energy
$G_k$	Generation of the turbulent kinetic energy
$I$	Turbulence intensity
$k$	Kinetic Energy
$M$	Turbulent Mach number
$P$	Mean pressure
$P_k$	Turbulent kinetic energy production rate due to mean velocity gradients
$P_b$	Turbulent kinetic energy production rate due to buoyancy
$Pr_t$	Turbulent Prandtl number for energy
$S$	Modulus of the mean rate of strain tensor
$U$	Mean flow velocity
$Y_M$	Dilation dissipation
$g$	Gravitational acceleration
$t$	Time

$\rho$	Mean density
$\beta$	Coefficient of thermal expansion
$g_i$	Gravitational vector
$u$	Velocity component in the x direction
$\mu$	Coefficient of viscosity
$\mu'$	Root-mean-square of the turbulent velocity fluctuations
$u_T$	Friction velocity
$\mu_t$	Turbulent viscosity
$v$	Velocity component in the y direction
$y$	Absolute distance closest to the wall
$w$	Velocity component in the z direction
$\varepsilon$	Rate of dissipation of kinetic energy

# 1. Introduction

## 1.1. Background

The UK and EU are committed to reduce greenhouse gas emissions by at least 80% in 2050 compared to emission levels in 1990. To achieve this ambitious target of 80% emissions reduction and transition to a low-carbon economy, the primary energy-demand sectors of focus are lighting and appliances, transport, industry, and heating and cooling (Department of Energy and Climate Change, 2010). The domestic sector is the second largest energy consumer, accounting for 28.9% of the UK's total energy consumption in 2018, across transport, industry, and services sectors (Department for BEIS, 2019). Space heating in domestic dwellings represents the largest energy consumption within this sector, amounting to approximately 61% (Jason Palmer and Cooper, 2012). Given the substantial energy usage in the domestic sector, it contributes significantly to greenhouse gas emissions.

Hammond and Stapleton (2001) found that electricity generation, domestic energy use and transport hold significant potential for efficiency improvements. Numerous approaches for enhancing energy systems efficiency have been proposed, and demand for even greater efficiency continue to grow. One viable method for improving efficiency is capturing and reusing wasted energy (Keirstead et al., 2012). In domestic building, space conditioning accounts for the majority of total energy consumption, with energy loss constituting more than half of the energy used for



space heating (Firth et al., 2019). Reducing and reusing energy loss is particularly crucial in the domestic sector, as the primary fuel for space heating and hot water is derived from fossil fuel (Palmer et al., 2012). Furthermore, issues such as overheating, cooling, condensation and excessive humidity affect energy consumption and indoor environment comfort, especially as building envelopes become tighter to conserve energy.

HVAC (heating, ventilation and air-conditioning) systems are integral to domestic buildings, serving to heat and cool internal occupied spaces, while providing acceptable indoor air quality (IAQ) and comfortable environment through ventilation. In domestic dwellings, air infiltration and natural ventilation are the primary ventilation method; however, these are considered less efficient in terms of energy savings for the building (Rhodes, 1995). Energy consumption of HVAC systems in building services accounts for 50% to 60% of the total energy consumption (Dimitroulopoulou, 2012; Ahmad et al., 2016). Conversely, mechanical ventilators play a critical role in a ventilation system by providing consistent, controllable ventilation. The application of heat recovery in mechanical ventilation can significantly reduce energy consumption in buildings (Dodoo et al., 2011). Nevertheless, they found that mechanical ventilation with heat recovery (VHR) system not only reduced energy consumption for space heating but also increased the electrical energy consumption for its operation.

Reducing energy consumption for space heating and cooling is a global challenge in achieving decarbonisation goals within the building sector. As a part of the

European Strategic Technology plan, the need of low-carbon technologies for heating and cooling utilising renewable energy sources has been highlighted in the recent years. The implementation of low-carbon ventilation technologies, such as powerless ventilators, presents a promising solution for reducing energy consumption in buildings (Tan et al., 2016). Powerless ventilators have the potential to facilitate ventilation, reduce energy consumption and improve IAQ by harnessing renewable energy sources, specifically wind (Lai, 2003; Khan et al., 2008a; Tan et al., 2016).

By applying of low-carbon ventilation technology, a reduction in of energy demand can be achieved through efficient supply using renewable energy resources. This research is driven by the path of the nearly zero-energy building (NZEB) programme established by the European Commission, contributing to the decarbonisation of heating and cooling in domestic dwellings. In accordance with Passivhaus standards, adopting a ventilation strategy is one of the key factors in achieving a Zero Carbon goal in building. Improving wellbeing and environmental health is another strong motivation of this study. Ensuring healthy IAQ is essential for addressing health concerns and preventing airborne disease transmission with an efficient ventilation system.

This study aims to investigate a novel concept of home ventilation systems integrated with a vertical axis wind turbine (see Figure 1.1). The proposed concept involves developing a new turbine ventilator design based on modifications to existing commercial wind-driven ventilators. This innovation turbine ventilator is

designed to facilitate ventilation for both supplying fresh air and exhausting stale air, setting it apart from most of commercial turbine ventilators, which primarily serve extract ventilation purposes (see Figure 1.2).

Despite the challenges associated with energy generation from small vertical wind turbines in urban areas – often limited due to the low speed of turbulent airflow (Drew et al., 2013; CORDIS, 2019) – this study aims to identify innovative solutions and design enhancements that can overcome these limitations. By addressing these challenges, the proposed ventilation system has the potential to significantly improve efficiency and sustainability, aligning with global decarbonisation goals and contributing to the development of NZEBs.

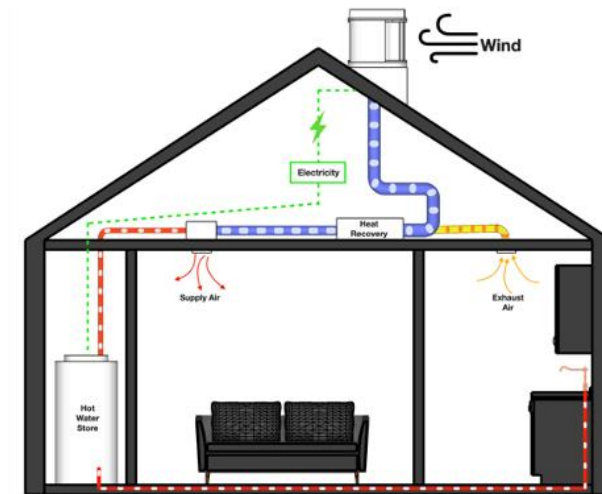


Figure 1.1. Schematic of concept of home ventilation system.



Figure 1.2. Wind-powered turbine Savonius (a) and Wind-powered fan VT turbine (b)  
(Ventilationland, 2021).

The utilisation of powerless turbine ventilator for inducing exhaust air flow through the roof has demonstrated effectiveness and efficiency in industrial buildings. However, their adoption in domestic ventilation systems has been limited, primarily due to concerns related to the required working environment, visual pollution for some homeowners, and the reliance on an inconsistent resource for operation. Consequently, these ventilators are often undervalued in ventilation strategies when compared to HVAC systems, which are perceived as more efficient in terms of energy savings and ventilation performance.

A potential solution lies in developing a novel ventilation system integrated with a low-carbon turbine ventilator that maximises natural wind energy for both ventilation and energy conservation purposes. Such innovation would offer a more cost-effective and sustainable option for residential buildings. By addressing the challenges inherent in traditional turbine ventilators and maximising the use of renewable energy sources, this cutting-edge approach could significantly reduce

energy consumption and emissions, while providing a compelling alternative for homeowners who prioritise the balance between comfort and environmental responsibility.

This study sets forth the hypothesis of developing an innovative home ventilation system that incorporates a wind-driven turbine ventilator as a key component, with the primary objectives of reducing energy consumption and enhancing indoor air quality in residential buildings. Drawing inspiration from fundamental principles of HVAC systems, the proposed ventilation system would possess the ability to supply fresh air and extract stale air simultaneously, eliminating the need for grid power and thus promoting energy efficiency.

## 1.2. Research Questions

As the present study concentrates on developing a numerical model to accurately simulate and predict the performance of the proposed turbine ventilator in terms of air supply and exhaust ventilation, a comprehensive understanding of the system's viability is crucial. To achieve this, the following research questions will be addressed:

Q1: How much air flow rate will the proposed turbine ventilator be able induce?

Q2: How effective will the proposed turbine ventilator be compared with the conventional ventilator?

Q3: Does the ventilation performance of the proposed turbine ventilator satisfy the Building Regulation's minimum requirement of ventilation rate?

Q4: Is the proposed turbine ventilator applicable to conventional dwellings?

## 1.3. Research Objectives

The primary objective of the present study is to explore the applicability of the turbine ventilator as a driver in HVAC system in terms of inducing power for ventilation.

The specific objectives of this study are as follows:

1.3.1 Create a three-dimensional computer-aided design (CAD) model for a Computational Fluid Dynamics (CFD) analysis.

1.3.2. Prepare a CFD model for meshing and simulation.

1.3.3. Conduct a validation of CFD results by comparing with other studies' data.

1.3.4. Quantify the influence of other features on performance improvements.

#### 1.4. Scope

This study is organized into six main sections, which are briefly described below:

1.4.2. **Introduction:** This section provides the background and motivation behind the study, addressing the issues of reducing energy consumption for spacing heating and improving indoor air quality through the use of wind-driven turbine ventilator. It also outlines the aim, research questions and objectives of the study.

1.4.3. **Literature Review:** This section delves into fundamental concepts and influences of ventilation systems on domestic dwellings. It covers a range of topics, including types of ventilation, ventilation strategy, influence on energy savings. The use of natural resource in ventilation systems and the adoption of low-carbon technologies are also discussed. A comprehensive review of wind-driven technology for domestic dwellings is carried out, along with an examination of the potential of turbine ventilators in domestic ventilation systems. Finally, the application of CFD modelling in this study and how to approach it was mentioned.

1.4.4. **Methodology:** This section describes the methodology implemented in the study, including the software used for CFD analysis, the physics

and turbulence modelling employed for simulations, and the overall approach to CFD simulation setup.

- 1.4.5. **Results and Discussion:** This section presents the results from CFD simulations, visualising flow characteristics and behaviour around and within the turbine ventilator. Several different configurations of the turbine ventilator are numerically tested and analysed, with their performances assessed in terms of ventilation rates. The results are compared to those from other studies, modifications are made to the turbine ventilator to explore and improve its ventilation performance.
- 1.4.6. **Conclusion:** This section summarises the overall findings of the study, addressing whether the research questions have been answered and providing an overview of the potential of the turbine ventilator when applied to buildings. Research limitations were also mentioned.
- 1.4.7. **Future Work:** This section offers recommendations for future research on this alternative home ventilation system, identifying areas that have not yet been explored and suggesting possible avenues for further investigation.



## 2. Literature Review

### 2.1. Influence of Ventilation Systems on Domestic Dwellings

Ventilation is a process that facilitates the exchange of air within building envelopes, ensuring occupant comfort by supplying fresh air and maintaining healthy indoor air quality (IAQ) through the dilution of air pollutants. Insufficient ventilation in buildings can adversely affect humidity, odours, pollutants, overheating, and condensation (Rhodes, 1995). Adequate ventilation is vital for domestic dwellings with concerns for health and comfort. As energy-efficient building envelopes become increasingly airtight to conserve energy, the potential for under-ventilation, resulting in poor IAQ and over-ventilation, leading to energy loss, becomes more prevalent (Russell et al., 2007). Ventilation systems are essential in creating optimal living conditions, considering IAQ and indoor thermal comfort.

Three distinct methods of ventilation are natural, mechanical and hybrid ventilation. Natural ventilation relies on natural forces, such as wind pressure and thermal buoyancy, to facilitate ventilate air infiltration through windows, powerless rotating ventilators, windcatchers, ventilation chimneys and windscoops. Mechanical ventilation, on the other hand, employs fan-powered systems used to supply and exhaust air from a space. Hybrid ventilation combines the features of both natural and mechanical systems, utilising natural forces for ventilation rates and switching to mechanical ventilation when natural forces are insufficient (Russell et al., 2007). Selecting an appropriate ventilation system is crucial, as it requires the consideration of factors such as desired IAQ, costs, heating and cooling loads and design

preferences (Dimitroulopoulou, 2012). The choice of a ventilation system can affect heating and cooling loads in domestic dwellings, ultimately influencing energy consumption and greenhouse gas emissions (Guillén-Lambea et al., 2016).

Heating and cooling loads represent one of the primary factors influencing residential energy consumption. According to a review by Pérez-Lombard et al. (2008), energy consumption by heating, ventilation and air-conditioning (HVAC) in UK residential buildings accounts for 62% of total energy consumption. Furthermore, HVAC systems in building services can consume 50% to 60% of total end-use energy (Ahmad et al., 2016). Consequently, the promotion of energy efficiency improvements is essential for minimising of energy consumption in buildings, which can be achieved through the implementation of more energy-efficient technologies and supportive government policies (Peter G. Taylor et al., 2010).

## 2.2. Applications of Ventilation Technology for Energy Efficiency

The demand for ventilation technologies extends beyond merely satisfying ventilation requirements, as they not only improve the indoor environment but also reduce energy consumption (Russell et al., 2007). In residential buildings, ensuring adequate ventilation rates is essential, as practical ventilation rates often fall below the standard regulations in European countries (Dimitroulopoulou, 2012). Dimitroulopoulou (2012) revealed that ventilation rates for a majority of the dwellings across Europe fall below a standard of  $0.5 h^{-1}$ , resulting in under-ventilation. Under-ventilation domestic buildings can pose health risks and create uncomfortable indoor environments for occupants. Implementing an energy-efficient ventilation system

can significantly impact IAQ improvements and energy savings when retrofitting a conventional or under-ventilated house (Hesaraki et al., 2015). Nonetheless, specific ventilation flow rates must be satisfied by any means of technology. According to regulations in England, the minimum requirement of whole-dwelling ventilation rate is 29 l/s for continuous ventilation of five bedrooms (Guillén-Lambea et al., 2016).

The influence of ventilation on energy use is significant, and the ventilation technologies play a crucial role in energy efficiency improvements concerning energy concerns. Ventilation systems, whether natural or mechanical supply/exhaust types, can significantly impact IAQ improvements and minimise energy consumption in domestic dwellings. However, the optimisation of ventilation systems typically depends on factors such as climate zones, heating and cooling demands and air quality requirement (Santos and Leal, 2012; Hesaraki et al., 2015; Guyot et al., 2018; Delwati et al., 2018; Zemitis and Borodinecs, 2019).

In terms of energy savings, energy recovery is an efficient solution within ventilation systems. A heat exchanger can be incorporated into any type of ventilation system, whether mechanical or natural, to harness heat from exhaust air and reuse it to precondition supply air (Russell et al., 2007). Guillén-Lambea et al. (2016) demonstrated that the regulations of European countries for ventilation rates are inconsistent with the energy demands of nearly zero-energy buildings without implementing heat recovery in ventilation systems. By integrating heat recovery into a mechanical ventilation system, it can significantly contribute to reducing primary energy use in buildings. Zemitis and Borodinecs (2019) showed that mechanical

ventilation systems with exhaust air heat recovery are capable of reducing heat consumption for a single-family house.

### 2.3. Natural Ventilation Systems in Building

Mechanical ventilation systems have been widely employed for IAQ improvements and reductions in energy consumption related to heating and cooling. A majority of newly constructed dwellings are installed with mechanical ventilation featuring heat recovery (Dimitroulopoulou, 2012). The primary reason for their popularity is the reliability and controllability of ventilation rates compared to natural ventilation, although their drawback is the additional energy consumption, specifically electricity, required for operation (Russell et al., 2007; Lai et al., 2018).

Natural ventilation systems primarily utilise the stack effect and wind-driven ventilation. Although newly built dwellings often take natural ventilation systems into consideration, the integration of advanced ventilation technologies is highly desirable for enhancing IAQ and reducing energy consumption (Russell et al., 2007). Given the environmental crisis and the need of low-carbon technologies and renewable energy resources, natural ventilation technologies, such as wind catchers and powerless rotating ventilators offer promising opportunities to address energy concerns while maintaining acceptable IAQ in residential buildings (Khan et al., 2008a). In terms of the renewable and green energy, these technologies possess advantages over mechanical ventilation systems, including cost-effectiveness and reduced carbon emissions through the use of renewable energy sources.

The integration of mechanical and natural ventilation systems, also known as hybrid systems, has gained increasing interest in recent years due to their ability to provide a high level of IAQ while minimising energy consumption. A combination of these two systems can be tailored to current ventilation systems, either by enhancing ventilation components or incorporating stack effects with mechanical ventilation systems (Russell et al., 2007; Khan et al., 2008a; Zhai et al., 2011). Cho et al. (2021) found that the application of a hybrid ventilation system is considered energy-efficient, as it can maintain good IAQ while consuming less energy during the heating season. Another study by Turner and Awbi (2014) demonstrated that a hybrid ventilation system, which combines primary natural ventilation with mechanical fan-powered devices, has the potential to satisfy heating and cooling demands and IAQ requirements in an energy-efficient manner. This evidence suggests that hybrid systems with a primary natural ventilation technique can achieve both energy efficiency and maintain good levels of IAQ for residential buildings.

#### 2.4. Wind-Driven Ventilation Technologies for Domestic Dwellings

The use of natural ventilation components as enhancements for ventilation systems has become increasingly desirable in the building sector. Low-carbon technologies such as windcatchers and turbine ventilators are commonly used in commercial, educational, and industrial buildings for cooling and ventilation purposes (Khan et al., 2008a). Powerless rotating or turbine ventilators are wind-driven air exhaust technologies that facilitate ventilation in domestic and industrial buildings (Khan et al., 2008b). Turbine ventilators are extensively utilised, particularly in warm

countries, as an exhaust ventilation system to alleviate poor IAQ and cooling loads in buildings, subsequently reducing energy consumption (Lai, 2003; Tan et al., 2016). As global temperature rise, energy consumption for increased cooling demands can be mitigated through the use of turbine ventilators. However, over-ventilation may pose an issue when employing this technology, as Streckienė et al. (2018) discovered that the volume of air exhausted in a building was 12 to 41% higher than required. Khan et al. (2008b) also pointed that using this technology could lead to energy losses in mild climate countries where heat conservation is necessary during winter. Although turbine ventilators represent an energy-efficient solution for buildings in warmer countries, there is a lack of robust studies on their application in ventilation systems for domestic buildings located in mild climate zones.

Another natural ventilation technology, windcatchers, is predominantly used in educational and industrial buildings to facilitate ventilation through wind and stack effect while reducing cooling loads. In mild climates, natural ventilation systems with heat recovery can be achieved using windcatchers integrated with heat exchangers (Saadatian et al., 2012; Calautit et al., 2020). An example of a windcatcher with a heat recovery system is Monodraught's Windcatcher HX, which is capable of delivering cooling ventilation and heat recovery (Monodraught, 2020). However, windcatchers have not been widely adopted when retrofitting conventional residential buildings (Khan et al., 2008a; Jomehzadeh et al., 2020).

## 2.5. Vertical Axis Wind Technology as Active Wind Driven Ventilation

Commercial turbine ventilators are typically designed in spherical or cylindrical shapes, equipped with curved or straight vertical vanes. The vanes are propelled by wind, which serves as a driving force, causing the turbine to rotate. This rotation generates a centrifugal force within the turbine, which in turn facilitates air extraction. However, the efficiency of these conventional type of the turbine ventilators tends to diminish under low wind speed conditions (Tan et al., 2016). In terms of noise emissions, turbine ventilators are generally known for their low acoustic levels during operation. For example, Bradford Ventilation's turbine ventilators have reported noise-emission levels ranging from 36.5 dB(A) to 60 dB(A) (Bradford Ventilation, 2023).

One proposed alternative to these conventional systems is the Savonius rotor, a drag-driven vertical wind turbine. A notable element of this design is its high starting torque, which function independently of the wind direction. When it comes to roof-mounted turbines, environmental factors such as noise and vibrations pose significant concerns, particularly in densely populated areas. These noise emissions and vibrations are known to have potential adverse impacts on urban residents. Savonius turbines, however, are considered for their low-level acoustic emissions and less vibrations (Akwa et al., 2012; Tahani et al., 2017; Noman et al., 2022). This makes them a suitable option for urban environments.

By adopting the Savonius turbine design, it offers an opportunity to enhance the overall performance and efficiency of the ventilation system through the integration of different turbine technologies. Moreover, by modifying the configuration of

conventional turbine ventilators, their performance can be improved, and environmental impacts such as noise emissions and vibrations can be minimised. Therefore, future research should focus on exploring these potential synergies and identifying optimal combinations of turbine technologies to maximise ventilation efficiency while minimising environmental impacts.

## 2.6. Potential of Turbine Ventilator in Domestic Ventilation System

The decarbonisation of the building sector has emerged as a critical area of focus, given its significant implications for greenhouse gas emissions reduction. Conventional mechanical ventilation systems generally consume electricity for their operation (Russell et al., 2007; Lai et al., 2018; Delwati et al., 2018), which underscores the pressing need for the development and adoption of more renewable and energy-efficient technologies. This has led to a growing interest in utilisation of natural forces for ventilation purposes.

Additionally, the importance of adequate ventilation has been highlighted by recent public health concerns, such as COVID-19 in crowded space (WHO, 2021). Turbine ventilators represent a promising solution in this regard, as they not only provide effective ventilation for buildings but also have potential to generate energy from renewable resources. However, a notable gap exists in the current body of research on the integration of turbine ventilators into balanced (supply and exhaust) ventilation systems with heat recovery that rely on renewable energy sources. Successful implementation of such systems could offer a more energy-efficient approach to ventilation in domestic buildings.



Given that wind-driven ventilation systems are contingent upon local wind conditions, and therefore subject to unbalanced ventilation rates, it is essential to consider supplementary energy sources for their operation. Several studies have explored the implementation of hybrid solar and wind ventilation systems (Lai, 2006; Shun and Ahmed, 2008; Shieh et al., 2010) and found that the combination of hybrid systems improved the stability of ventilation performance during periods of low wind speed. With redundancy considered, particularly in the wind-driven ventilation systems, it can significantly enhance energy efficiency and the overall performance of turbine ventilators.

## 2.7. Application of Computational Fluid Dynamics Approach

Wind tunnel testing is the commonly used techniques in aerodynamic studies to investigate wind characteristics and their effects on a particular object under specific conditions. However, traditional wind tunnel studies are considered costly and time consuming to achieve high accuracy and precision. Computational fluid dynamics (CFD) has emerged as an alternative for aerodynamic studies due to the decreasing cost-to-performance ratio of powerful computation, making it cost-effective (Lien and Ahmed, 2010).

Computational fluid dynamics (CFD) modelling has become a popular approach for wind investigations at an early design stage, as it is considered more economical and powerful in terms of costs and accurate predictions compared to physical wind tunnel experiments. The CFD approach has been adopted in many studies of turbine ventilators to simulate and analyse flow characteristics, including force, flow pattern,

and dynamic pressure (Lien and Ahmed, 2010; Lin et al., 2010; Adam et al., 2010; Jadhav et al., 2016). This allows to visualise detailed flow behaviour and provide deeper insight into the flow field without the need for testing costly physical prototypes. Lien and Ahmed (2010) highlighted the use of CFD analysis as a cost-effective aid for design optimisation and development of turbine ventilator.

Selecting an appropriate turbulence model in CFD numerical simulations is crucial as it needs to solve complexity of air flow behaviour around and within an object. Several studies found that standard k-epsilon turbulence model was proficient in providing reasonable estimates of the turbulent flow field around a complex geometry (Zhou and Stathopoulos, 1997; Adam et al., 2010; Lien and Ahmed, 2010). The standard k-epsilon model is governed by the Reynolds Averaged Navier Stokes (RANS) two equations, which is the most economical computation solution in terms of computational costs in CFD analysis. The standard k-epsilon model was an ideal choice for the present study, considering the requirement for relatively low computational resources for CFD simulation.

However, the standard k-epsilon model is considered inferior in predicting complex flows involving adverse gradients and flow separation (Zhou and Stathopoulos, 1997). Adam et al. (2010) and Chen et al. (2019) indicated that the application of the realisable k-epsilon turbulence model yielded more accurate capture of complex flows near the wall region, involving rotation, recirculation and boundary layer separation.

CFD modelling was conducted according to the Australian/New Zealand AS/NZS 4740:2000 standard, which prescribes test performance methods for natural ventilators (see Figure 2.1). This standard has been widely recognised and employed in the analysis of natural ventilation systems, providing a reliable and consistent basis for evaluation. Jadhav et al. (2016) also used the same standard for their test performance of the turbine ventilator models in both computational and physical experiments (see Figure 2.2). They reported that the error of CFD results compared to experimental data ranged from 12% to 15%, indicating a reasonably high degree of accuracy in their simulations.

In an effort to maintain consistency with the existing literature and ensure the reliability of the result, the computational approach for CFD simulation adopted by Jadhav et al. (2016) has been employed in this study. This approach enables a comprehensive examination of the flow characteristics, pressure distribution, and overall efficiency of turbine ventilators in various configurations, providing valuable insights into their potential for energy-efficient applications to domestic buildings.

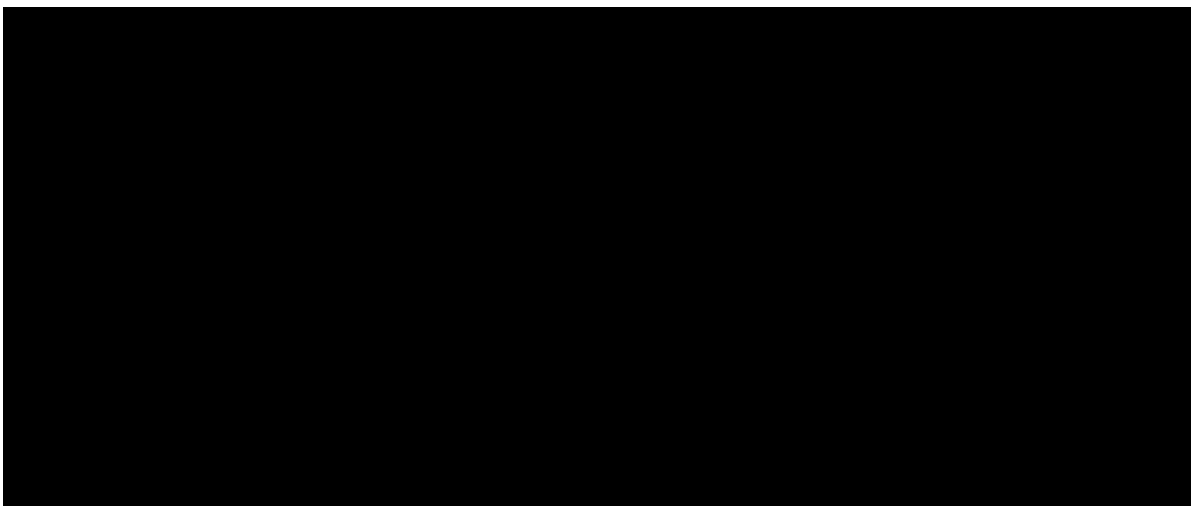


Figure 2.1. Schematic diagram of physical experiment setup (Khan et al., 2008a).

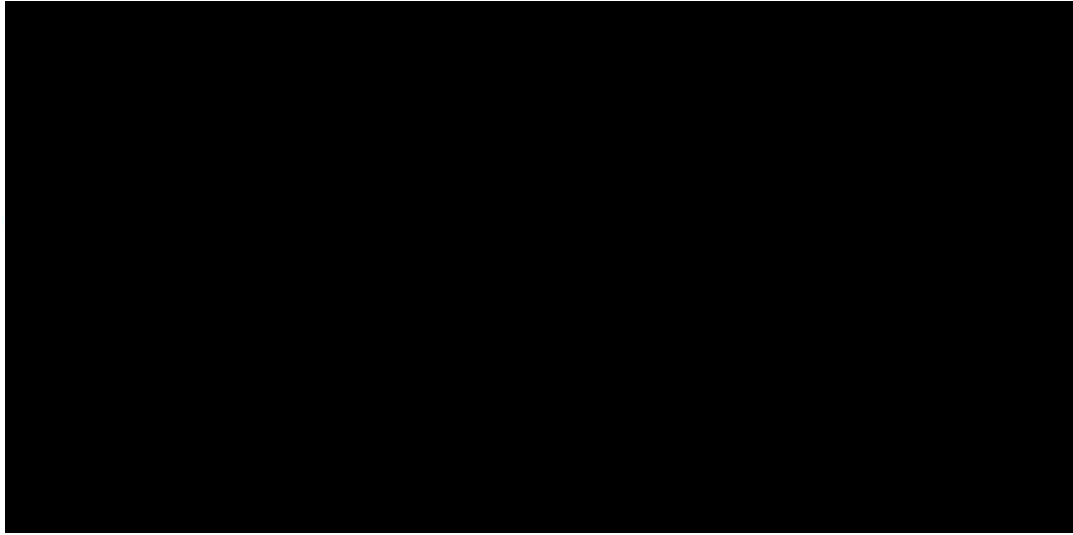


Figure 2.2. Computational domain for CFD simulation (Jadhav et al., 2016).

### 3. Methodology

The primary objective of this study is to investigate the potential of energy savings in domestic heating and cooling systems by integrating a novel home ventilation concept with the use of powerless roof-mounted turbine ventilator. To achieve this goal, the Computational Fluid Dynamics (CFD) approach was adopted as an efficient and powerful tool for solving and analysing fluid flow problems.

The CFD analysis consists of three main phases: pre-processing, solving, and post-processing. During the pre-processing phase, input data is transformed into a discretised computational model. This involves preparing the geometry, defining physical model, setting initial/boundary conditions, and generating a mesh. The solving phase entails the application of numerical algorithms to solve complex fluid flow problems, incorporating the appropriate turbulence models and numerical

schemes. Lastly, the post-processing phase focuses on interpreting and visualising the results through various methods such as graphs, vector plot, contour plot, or streamline.

In the study, two Computational Fluid Dynamics (CFD) modelling software platforms, SimScale and Autodesk CFD, were employed to analyse and visualise fluid flow patterns and behaviour of a turbine ventilator. SimScale is an online browser-based software platform that specialises in engineering modelling and simulations for fluid dynamics and thermodynamics (SIMSCALE, 2020). This platform offers an advanced numerical approach of rotating zone simulations for ventilators, which is essential for the accurate representation of the turbine ventilator's performance. Autodesk CFD, on the other hand, provides a comprehensive suite of powerful tools for fluid flow prediction and is widely recognised for its robustness and versatility in handling complex flow problems (Autodesk CFD, 2019). Figure 3.1 illustrates the overall CFD methodology applied in the study, highlighting the key steps and processes involved in the CFD modelling.

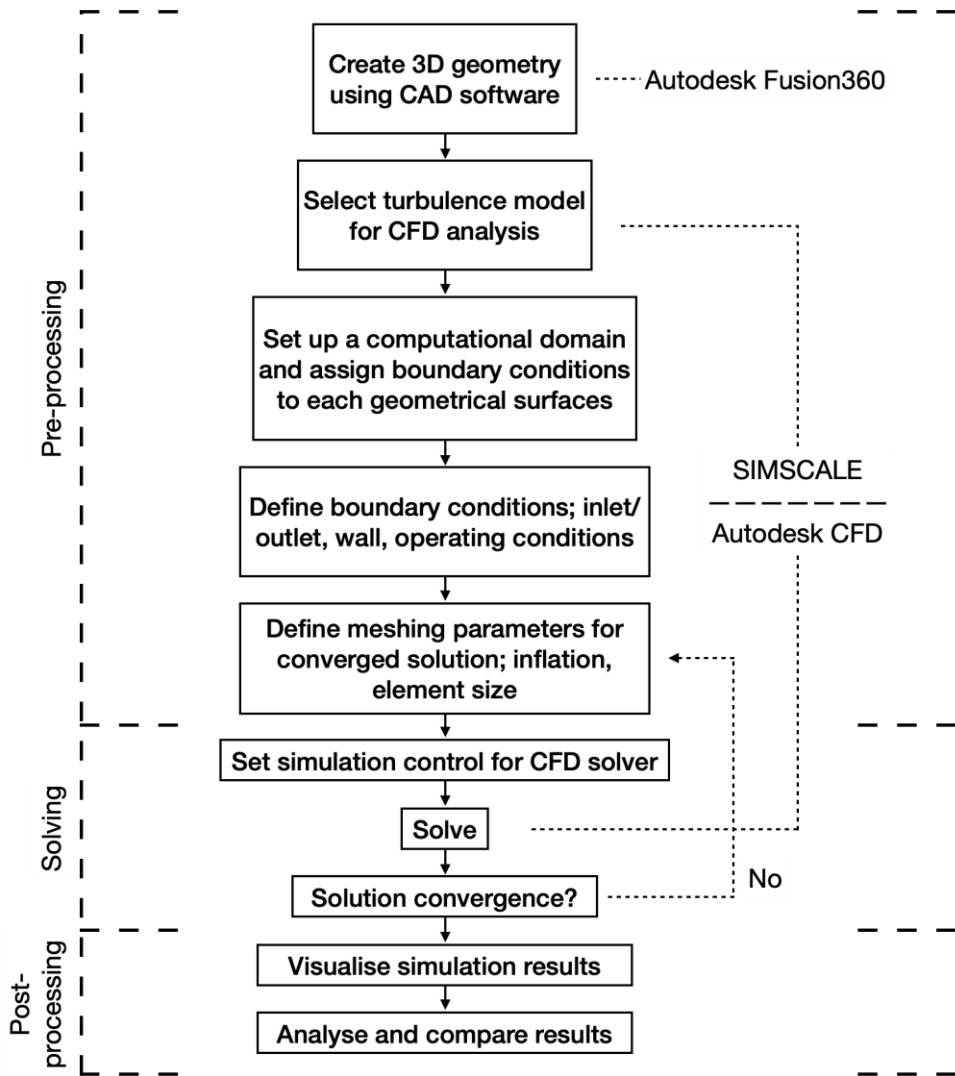


Figure 3.1. Flowchart of method for application of CFD simulation.

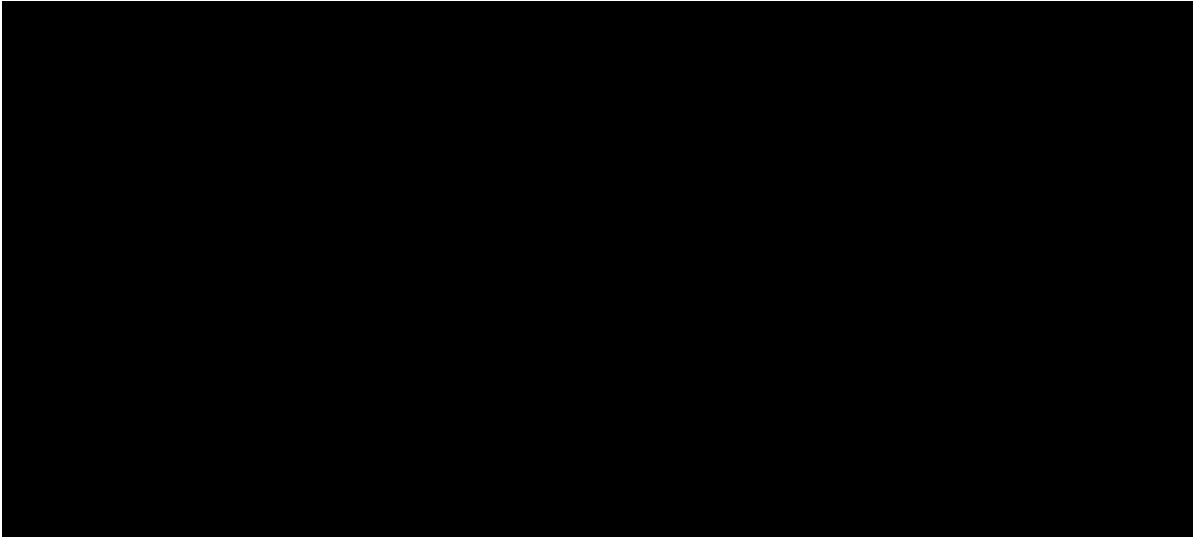
### 3.1. Modelling Turbine Ventilator

The integration of a wind-driven turbine ventilator into a ventilation system is an innovative concept, as depicted in Figure 1.1. The design of this novel turbine ventilator draws inspiration from the Savonius vertical axis wind turbine and existing commercial wind-driven ventilation technologies, as shown in Figure 1.2. The Savonius turbine offers numerous advantages, including a straightforward mechanism, low operation noise, excellent self-starting capability, and

independence from wind direction (Akwa et al., 2012; Tahani et al., 2017). Furthermore, it is well-suited for distributed energy generation in low-demand scenarios, heating, ventilation, and air-conditioning (HVAC) applications in buildings and hybrid renewable energy systems.

Currently, turbine ventilators on the market are primarily employed in exhaust ventilation systems for various types of buildings. The extract ventilation rates of these turbine ventilators depend on factors such as size and wind speed. The performance of these commercial ventilation technologies is detailed in Table 3.1.

Table 3.1. Commercial turbine ventilation technologies (Ventilationland, 2021).



Research conducted by Lai (2003) and Khan et al. (2008b) demonstrated that larger turbine ventilators yield improved ventilation rates. Despite this finding, Lai (2003) recommended an optimal size for open duct turbine ventilator to be between 0.36 and 0.5 diameter, as the ventilation performance remains relatively consistent within this range. Moreover, other critical parameters that influence the capacity of flow rate include the throat diameter, construction material of the turbine ventilator, and blade design.

To optimise the efficiency of the proposed turbine ventilator, it is essential to consider these key parameters during the design process. Consequently, an in-depth review of relevant literature (Akwa et al., 2012; Tahani et al., 2017; Lai, 2003; Khan et al., 2008b) was conducted to identify best practices and refine the turbine ventilator's design. By merging these insights, the proposed turbine ventilator will not only exhibit enhanced performance, but it will also contribute to the advancement of more sustainable and energy-efficient ventilation systems within the building sector. This innovative approach aligns with current trends towards decarbonisation and energy conservation in the built environment, ultimately promoting a more sustainable future.

Moreover, considering the limitations of commercial ventilators in supplying fresh air to buildings, this study proposes a new design for a turbine ventilator capable of facilitating a balanced ventilation system. The key design parameters from the existing studies were considered during the modelling process of the turbine ventilator.

A turbine ventilator model was developed using Autodesk Fusion 360, a powerful three-dimensional CAD software offering advanced technical design tools within



intuitive interface, enabling swift creation and modification of 3D models. The 3D model of the turbine ventilator, consisting of a fresh air intake vent and a turbine extractor, was created and exported to a CFD software for meshing and CFD simulation (see Figure 3.2). The proposed turbine ventilator operates based on active and passive wind-driven ventilation strategies, employing the air intake vent to supply fresh air into a building and utilising the rotating turbine to extract stale air (see Figure 3.3a). The rotational motion of the turbine blades generates a negative pressure field within the turbine, resulting in suction effects that facilitate air extraction from the duct.

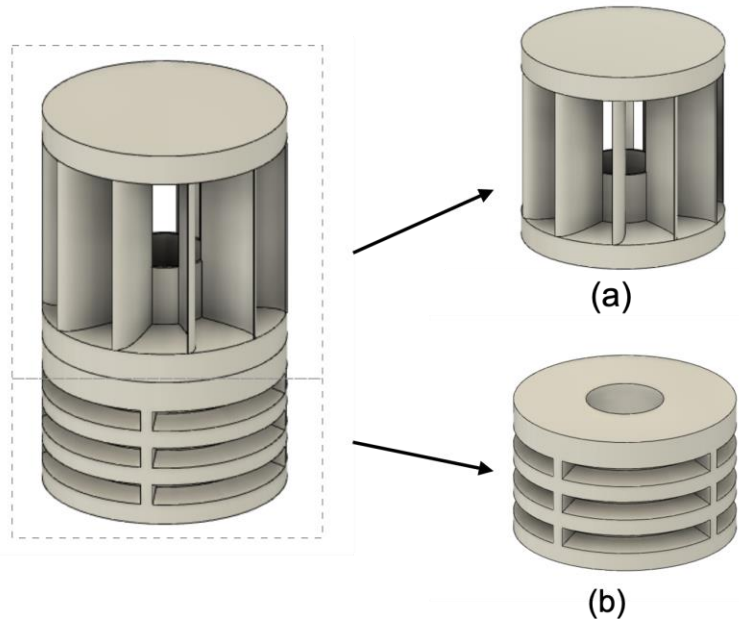


Figure 3.2. Turbine ventilator model: (a) turbine air extractor and (b) fresh air intake vent.

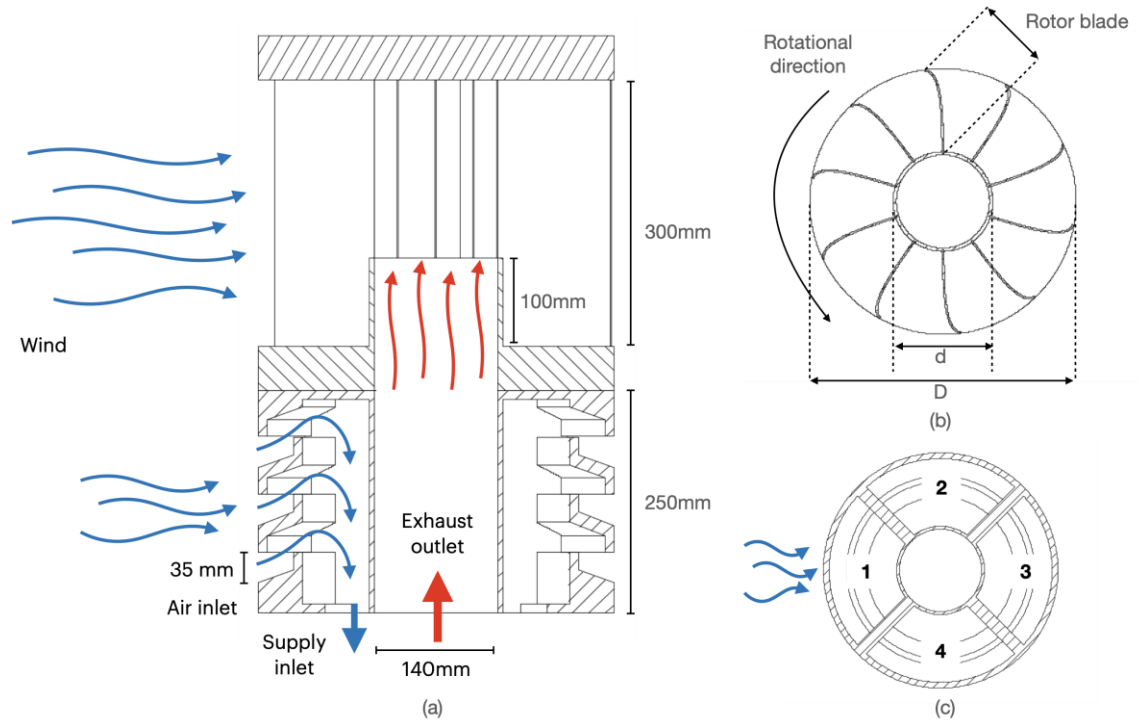


Figure 3.3. Schematic: (a) principle of the proposed turbine ventilator, (b) the geometrical parameters of the rotor domain and (c) air intake vent.

Blade configuration, throat diameter and construction material are the key parameters that significantly influence the performance of a turbine ventilator (Khan et al., 2008b). The geometry of the turbine rotor domain is illustrated in Figure 3.2b, with the turbine diameter ( $D$ ) measuring 400mm and the duct size ( $d$ ) at 140mm. Alom and Saha (2019) found that an elliptical blade profile exhibited superior rotor performance compared to semi-circular, Benesh and modified Bach rotors, with improvements of 20.25%, 19.49% and 17.28% respectively. Consequently, the elliptical blade profile was adopted, featuring a blade height of 300mm and an exhaust duct extending 75mm from the rotor base. The air intake vent was designed to be 250mm high, with a 35mm gap between louvers, allowing fresh air entry into the building. A circular air intake vent with four openings was modelled (See Figure

3.3c). This innovative design is anticipated to enhance ventilation efficiency, contributing to energy savings and improved indoor air quality.

### 3.2. Turbulence Modelling

The present study employed a steady-state Reynolds-Averaged Navier-Stokes (RANS) solver for CFD simulations, which aimed to investigate the flow characteristics of the turbine ventilator. As a numerical method, steady-state RANS computes time-independent flows by decomposing them into time-averaged and fluctuating quantities. This method offers the advantage of significantly reducing the computational resources required for simulations under steady-state conditions (Baker et al., 2019). The governing equations for three-dimensional incompressible flows, as given by steady-state RANS equations, are based on the conservation law of mass (Continuity) and momentum. The equations for three-dimensional flows in x, y and z coordinates are as follows (SIMSCALE, 2020):

Continuity Equation

$$\frac{\partial \rho u}{\partial x} + \frac{\partial \rho v}{\partial y} + \frac{\partial \rho w}{\partial z} = 0 \quad (3.1)$$

X-Momentum Equation

$$\rho \left( \frac{\partial u}{\partial t} + u \frac{\partial u}{\partial x} + v \frac{\partial u}{\partial y} + w \frac{\partial u}{\partial z} \right) = \rho g_x - \frac{\partial P}{\partial x} + \mu \left( u \frac{\partial^2 u}{\partial x^2} + v \frac{\partial^2 u}{\partial y^2} + w \frac{\partial^2 u}{\partial z^2} \right) \quad (3.2)$$

### Y-Momentum Equation

$$\rho \left( \frac{\partial u}{\partial t} + u \frac{\partial v}{\partial x} + v \frac{\partial v}{\partial y} + w \frac{\partial v}{\partial z} \right) = \rho g_y - \frac{\partial P}{\partial x} + \mu \left( u \frac{\partial^2 u}{\partial x^2} + v \frac{\partial^2 u}{\partial y^2} + w \frac{\partial^2 u}{\partial z^2} \right) \quad (3.3)$$

### Z-Momentum Equation

$$\rho \left( \frac{\partial u}{\partial t} + u \frac{\partial w}{\partial x} + v \frac{\partial w}{\partial y} + w \frac{\partial w}{\partial z} \right) = \rho g_z - \frac{\partial P}{\partial x} + \mu \left( u \frac{\partial^2 u}{\partial x^2} + v \frac{\partial^2 u}{\partial y^2} + w \frac{\partial^2 u}{\partial z^2} \right) \quad (3.4)$$

The terms of  $u$ ,  $v$ , and  $w$  in the continuity equation are defined as the velocity components of the  $x$ ,  $y$  and  $z$  coordinates respectively. Where  $\rho$  is the mean density and  $g$  represent the gravitational acceleration, by combing these two, the gravitational force is given.  $t$  represents the time and  $P$  is the mean pressure, whereas the coefficient of viscosity,  $\mu$  is constant.

Turbulence modelling plays a crucial role in CFD analysis by ensuring accurate and reliable prediction of wind flow phenomena. In conjunction with RANS equations, turbulence models are employed as a numerical approach that describe the development of oscillations in the turbulent flow transition. One such model, the k-epsilon model, is widely used and recognised for its robustness in efficiently simulating a broad range of mean flow characteristics for turbulent flow conditions with reasonable accuracy. The standard k-epsilon turbulence model based on RANS was adopted in practical applications of many studies due to its good convergence and relatively low computation cost, which provides reasonable estimate of complex flows through and around the turbine ventilator (Lien and Ahmed, 2010; Jadhav et

al., 2016; Lan et al., 2021). The standard k-epsilon model is based on two transport equations for the turbulence kinetic energy,  $k$  and its rate of dissipation,  $\varepsilon$  as follows:

For the kinetic energy,  $k$

$$\frac{\partial}{\partial t}(\rho k) + \frac{\partial}{\partial x_i}(\rho k u_i) = \frac{\partial}{\partial x_j} \left[ \left( \mu + \frac{\mu_t}{\sigma_k} \right) \frac{\partial k}{\partial x_j} \right] + P_k + P_b - \rho \varepsilon - Y_M + S_k \quad (3.5)$$

For the rate of dissipation,  $\varepsilon$

$$\frac{\partial}{\partial t}(\rho \varepsilon) + \frac{\partial}{\partial x_i}(\rho \varepsilon u_i) = \frac{\partial}{\partial x_j} \left[ \left( \mu + \frac{\mu_t}{\sigma_\varepsilon} \right) \frac{\partial \varepsilon}{\partial x_j} \right] + C_{1\varepsilon} \frac{\varepsilon}{k} (P_k + C_{3\varepsilon} P_b) - C_{2\varepsilon} \rho \frac{\varepsilon^2}{k} + S_\varepsilon \quad (3.6)$$

Where  $P_k$  is defined as the turbulent kinetic energy production rate due to mean velocity gradients,  $P_b$  represents the turbulent kinetic energy production rate due to buoyancy, and  $Y_M$  is the fluctuating dilation in compressible turbulence contributed to the overall dissipation rate.  $C_{1\varepsilon}$ ,  $C_{2\varepsilon}$ ,  $\sigma_k$  and  $\sigma_\varepsilon$  are constants with values of 1.44, 1.92, 1 and 1.3 respectively.  $S_k$  and  $S_\varepsilon$  are source terms defined by user.

The turbulent viscosity,  $\mu_t$  is obtained by the following equation:

$$\mu_t = \rho C_\mu \frac{k^2}{\varepsilon} \quad (3.7)$$

Where the equations for  $k$  and  $\varepsilon$  are expressed as follows (SIMSCALE, 2020):

$$k = \frac{3}{2} (UI)^2 \quad (3.8)$$

$$\varepsilon = C_\mu^{\frac{3}{4}} \cdot \frac{k^{\frac{3}{2}}}{l} \quad (3.9)$$

Where  $C_\mu$  is the empirical constant and takes the value of 0.09,  $U$  represent the mean flow velocity and  $I$  is the turbulence intensity which is defined as follows:

$$I = \mu' / U \quad (3.10)$$

Where  $\mu'$  is the root-mean-square of the turbulent velocity fluctuations, can be obtained by:

$$\mu' = \sqrt{\frac{1}{3}(\mu'^2_x + \mu'^2_y + \mu'^2_z)} = \sqrt{\frac{2}{3}k} \quad (3.11)$$

The mean velocity  $U$  can be calculated with the following equation:

$$U = \sqrt{U_x^2 + U_y^2 + U_z^2} \quad (3.12)$$

The term of the generation of the turbulent kinetic energy,  $G_k$  is defined as follows:

$$G_k = \mu S^2 \quad (3.12)$$

Where  $S$  is the modulus of the mean rate of strain tensor, which is expressed as the following:

$$S = \sqrt{2S_{ij}S_{ij}} \quad (3.13)$$

With the effect of buoyancy, the production of the turbulent kinetic energy,  $G_b$  is defined as the following equation:

$$G_b = \beta g_i \frac{\mu_i}{Pr_t} \frac{\partial T}{\partial x_i} \quad (3.14)$$

Where  $Pr_t$  is the turbulent Prandtl number for energy and  $g_i$  represents the gravitational vector in the  $i^{th}$  direction. The coefficient of thermal expansion,  $\beta$  is defined as follows:

$$\beta = -\frac{1}{\rho} \left( \frac{\partial \rho}{\partial T} \right)_p \quad (3.15)$$

The term of the dilation dissipation,  $Y_M$  is used to account for the compressibility effects on turbulent flows, which can be expressed as the following equation:

$$Y_M = 2\rho\varepsilon M^2 \quad (3.16)$$

Where M represents the turbulent Mach number that is defined as:

$$M = \sqrt{\frac{k}{a^2}} \quad (3.17)$$

The solver employed a discretisation-based method integrating an upwind and linear numerical scheme that includes first-order upwind and second-order upwind schemes to ensure the accuracy and stability of numerical solutions. This approach allowed for obtaining approximate solutions in a simple and computationally efficient way with minimal compromises in numerical accuracy. Furthermore, the application of the second-order upwind scheme, which considers the impact of two upstream nodes, substantially improves the reliability and accuracy of the simulation results.

However, it is important to note that Adam et al. (2010) and Zhou and Rempfer (2013) suggested that the realisable k-epsilon turbulence model outperformed the standard k-epsilon model in terms of capturing separated flows more accurately.

Nevertheless, due to the unavailability of the realisable k-epsilon turbulence model on SimScale and Autodesk CFD, the present study employed the standard k-epsilon turbulence model for CFD simulation.

### 3.3. Computational Domain

Utilising a CFD simulation approach, the wind tunnel domain setup for numerical simulations is based on the methodology presented by Jadhav et al. (2016). This method replicates the physical test rig employed in wind tunnel experiments. The computational domain consists of two main regions: the flow domain, which facilitates simulations of wind flow around the geometry of interest, and the chamber region, which enables the measurement of volume flow rates for the proposed turbine ventilator (see Figure 3.4). The dimensions of the computational domain were chosen to allow upstream flow to fully develop in the presence of the turbine ventilator geometry, while minimising the impact of the boundaries on the flow regime. The domain is divided into stationary, inner, and rotation sections.



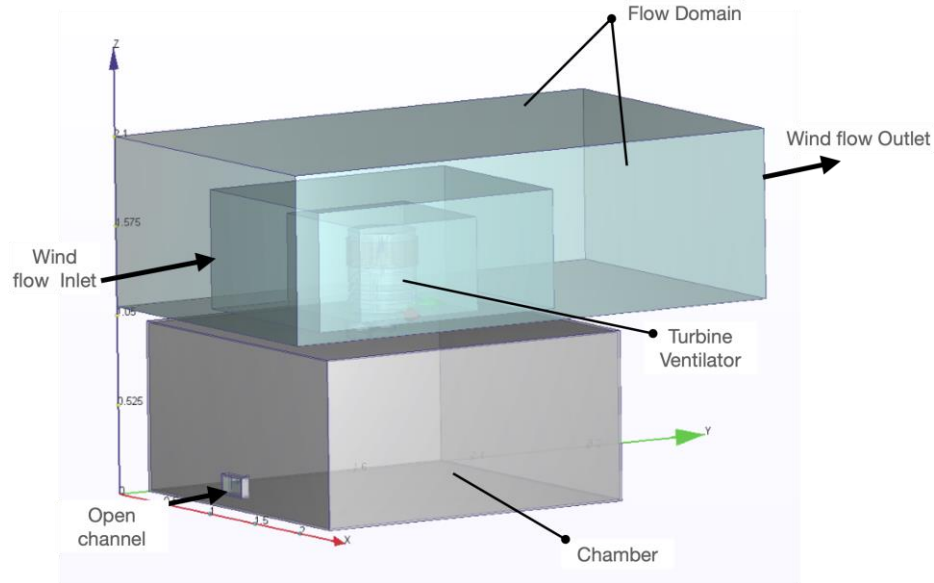


Figure 3.4. CFD computational doamin setup.

Domain sizing is vital for the CFD simulation process as it may significantly impact on solution accuracy and computational cost. Optimising a computational domain allows for the flow field to sufficiently develop around the body on interest and reduction in mesh density. The importance of numerical schemes has significant influences on the optimisation of a computational domain size. As an upwind numerical scheme was chosen, it has its own advantage in smoothing out solutions without the necessity of a large computational domain (Patankar, 1980). However, availability of computational resources is also one critical aspect to take into account in the domain optimisation process. The best practice guidelines set out by Franke and Baklanov (2007) has been recognised as one of the commonly adopted guidelines used for CFD simulation. Given that, a domain optimisation study by Abu-Zidan et al. (2021) provided the recommendation of smaller domain dimensions with an acceptable level of domain error based on Franke and Baklanov's guidelines. The

implementation of these guidelines would greatly assist in guiding the domain optimisation process in this study.

In this study, a domain convergence analysis was performed to find the optimal domain size that could capture the relevant flow behaviour. The computational domain optimisation was based on several criteria ensuring adequate distance from the boundaries to prevent any unwanted interference on the flow field. Abu-Zidan et al. (2021) found that computational domain dimensions could be minimised to a smaller size without any significant influence of the domain on solution accuracy, which in turn, would achieve savings in computational cost from uneconomic grids.

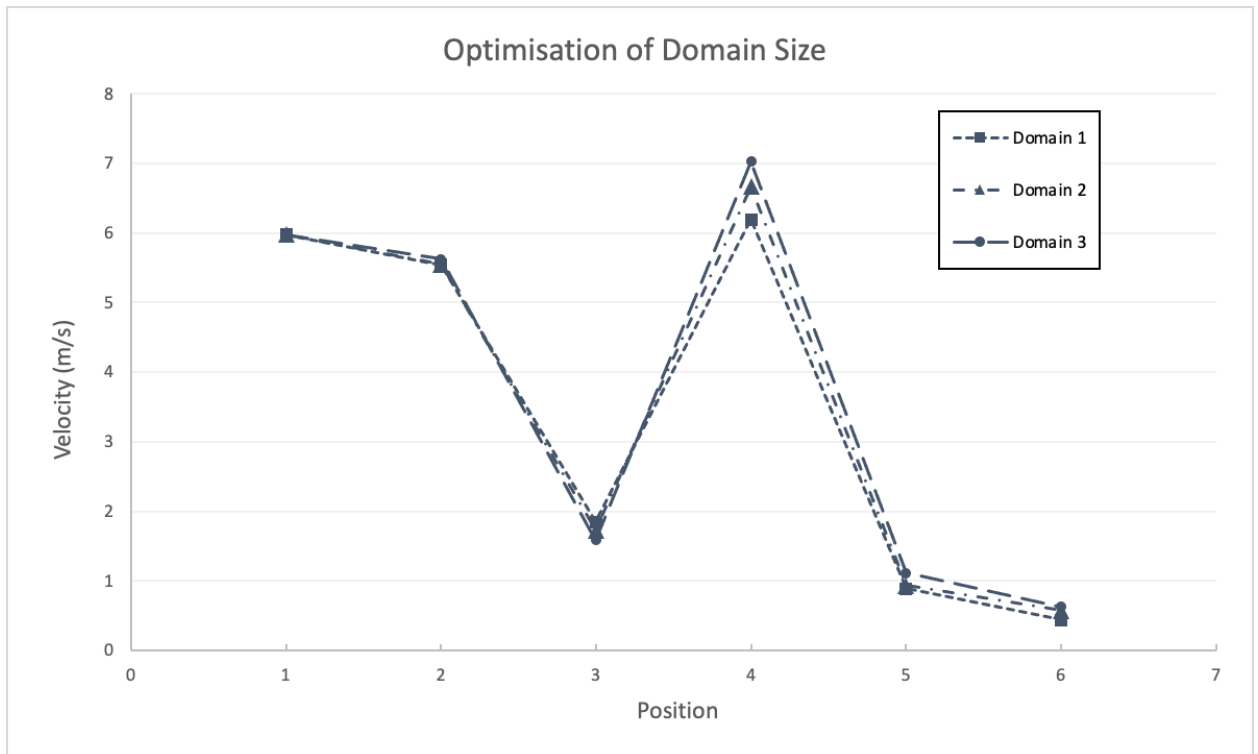


Figure 3.5. Comparison of the computational domain optimisation between different sizes.

To find an optimal domain size, three different domain sizes were considered in the parametric analysis. A preliminary size of computational domain was based on the guidelines, in consideration of the diameter of the turbine ventilator, domain parameters; upstream = 3D, downstream = 5D, width = 3D and height = 4D. To further explore other choices of the domain size, the domain was refined into smaller domains; reducing the width to 2.5D and height 2.5D for Domain 2; and decreasing a domain height to 2D for Domain 3. As a result, velocity magnitudes of the three computational domains were captured and plotted as shown in Figure 3.5. The maximum percentage errors of Domain 1 between Domain 2 and 3 was approximately 4.82% and 5.63% respectively (see Figure A1); however, considering computational resources required, the core hours of Domain 1,2 and 3 used were 91.04, 72.62 and 69.48 respectively. Since computational resources were limited, the dimensions of Domain 2 were therefore adopted in this study that could save around 20.2% on computational costs without a significant sacrifice of solution accuracy.

With the chosen domain dimensions, a similar size of the computational domain was also utilised in other studies (Lien and Ahmed, 2010; Ghanegaonkar et al., 2018). These studies presented the results on the same trend. Moreover, Anbarsooz (2016) implemented a similar size of a computational domain and showed the simulation results that were in agreement with the experimental results. Additionally, in order to improve its reliability in solution accuracy, an adaptive meshing technique was utilised to refine mesh cells in necessary regions, keeping the overall number of cells under control and obtaining accurate solution fields. Hence, the optimised size of the

computational domain is 3D upstream, 5D downstream, extending to a width of 2.5D for both right and left side boundaries, and a height of 2.5D, where D represents the diameter of the turbine ventilator (see Figure 3.6). The chamber dimensions are 2m wide, 2m long, and 1m high. These optimised dimensions could effectively address the aerodynamics issues related to the impact of geometry on the surrounding flow field.

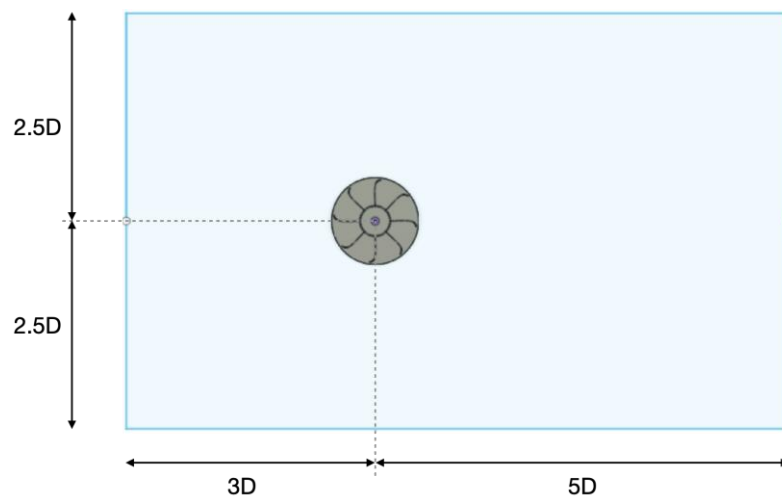


Figure 3.6. Modelling of computational domain.

### 3.4. Boundary Conditions

Figure 3.7 illustrates the assignment of boundary conditions to each face of the computational domain. The upstream entry of the computational domain was characterised as a uniform velocity-inlet boundary condition. The inflow rates encompassed a range of velocity magnitudes, specifically 1, 2, 3, 4, 5 and 6 m/s, which applied in the simulation. The rotation of turbine ventilators commenced when the wind speed exceeded 2 m/s (Rimdžius et al., 2018; Chen et al., 2019). A

pressure outlet boundary condition was designated for the domain's downstream end, adjacent turbine ventilator, where the pressure was set to 0.

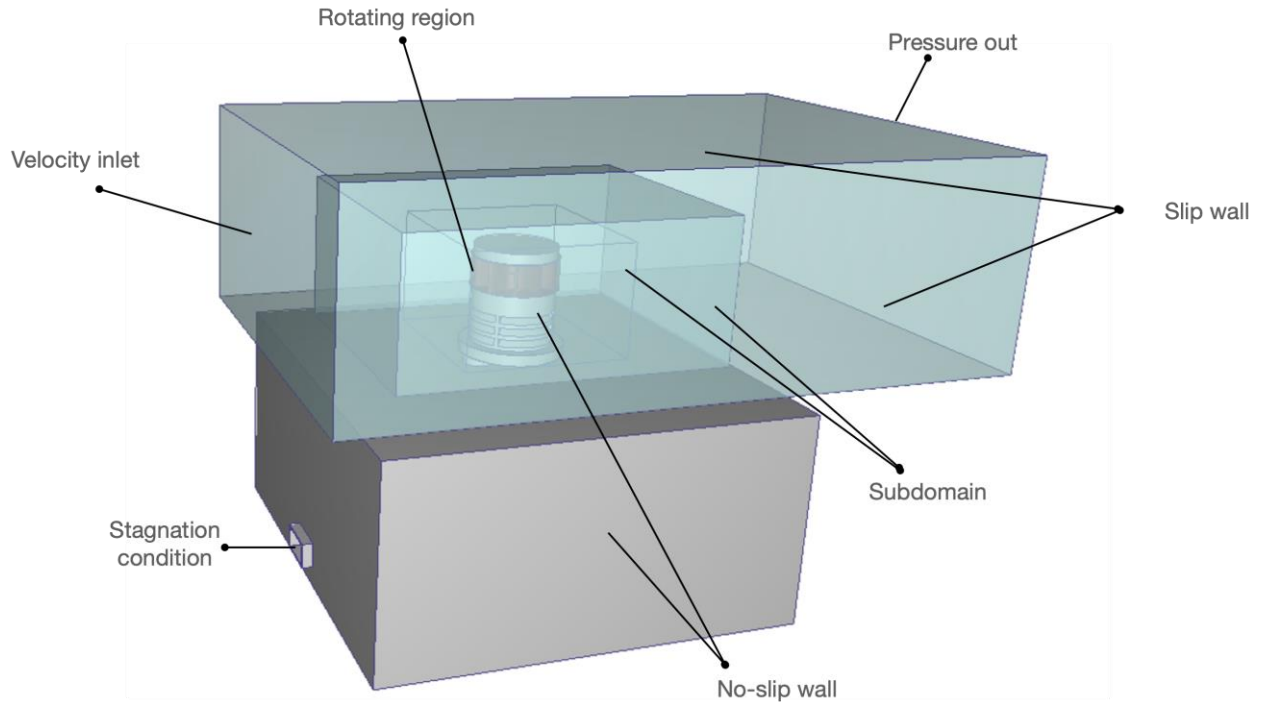


Figure 3.7. Boundary conditions

The lateral and top boundaries of the computational domain were defined as slip boundary condition, allowing the flows to slip along the boundaries and diminish. A no-slip wall boundary condition was imposed on the surfaces of the turbine ventilator, chamber, and bottom base of the computational domain. To capture the flow characteristics of the rotating turbine ventilator, the rotation domain was identified as a rotating region.

Considering that turbine ventilators typically operate in low wind speed environments, various rotational speeds corresponding to wind flow velocities were applied in the simulation. The present study's CFD simulation adopted rotational

speeds from the experimental results of the other studies (Khan et al., 2008b; Lien and Ahmed, 2011; Rimdžius et al., 2018) for the turbine ventilator. Table 3.2 displays the rotational speeds applied in the simulation setting according to the wind speed.

Table 3.2. Rotational speeds for CFD simulation.

Velocity (m/s)	Rotation speed (RPM)
1	48
2	60
3	115
4	167
5	216
6	267

### 3.5. Mesh Generation

In order to address the complex geometry, a combination of Hexahedral and Tetrahedral meshing was employed to capture the flow characteristics near the geometry of interest and to ensure the cell skewness remained less than 1 and close to 0. The maximum skewness of the mesh was targeted to be equal to or less than 0.85 for a high-quality mesh (Lien and Ahmed, 2010; Ghanegaonkar et al., 2018; SIMSCALE, 2020). Moreover, to maintain high mesh quality, the ideal aspect ratio of Hexahedral and Tetrahedral cells should be equivalent to 1 and 4, respectively. SimScale's recommendation for CFD analysis is an aspect ratio less than 10. The unstructured tetrahedral meshing was generated using the mesh generation tool by SIMSCALE (see Figure 3.8). Autodesk CFD was utilised as an alternative solution

for meshing and simulations. The multiple frame reference (MFR) approach was adopted to approximate the transient rotating motion of the turbine ventilator under steady-state conditions (Lien and Ahmed, 2010). The approach allows the simulation of rotation effects in the flow by incorporating these reference frames into a rotating region using the equations of a rotating governing frame.

In order to achieve a superior prediction of turbulent flows in the near wall region, a near-wall function approach was adopted with a value of  $y^+$  equal to or less than 1 (Zhou and Rempfer, 2013). The desired  $y^+$  value was obtained by calculating the dimensionless wall distance, which determined the thickness of the first wall boundary layer. The equation for estimating of the dimensionless  $y^+$  wall distance is expressed as follows:

$$y^+ = \frac{y \cdot u_\tau}{\nu} \quad (3.18)$$

Where  $u_\tau$  is the friction velocity,  $y$  is the absolute distance closest to the wall and  $\nu$  is the kinematic viscosity. Inflation boundary layers were generated with the first layer thickness of  $y^+ \sim 1$  and a growth rate of 1.3 (see Figure 3.8c). This allows to capture effects of a boundary layer separation accurately.

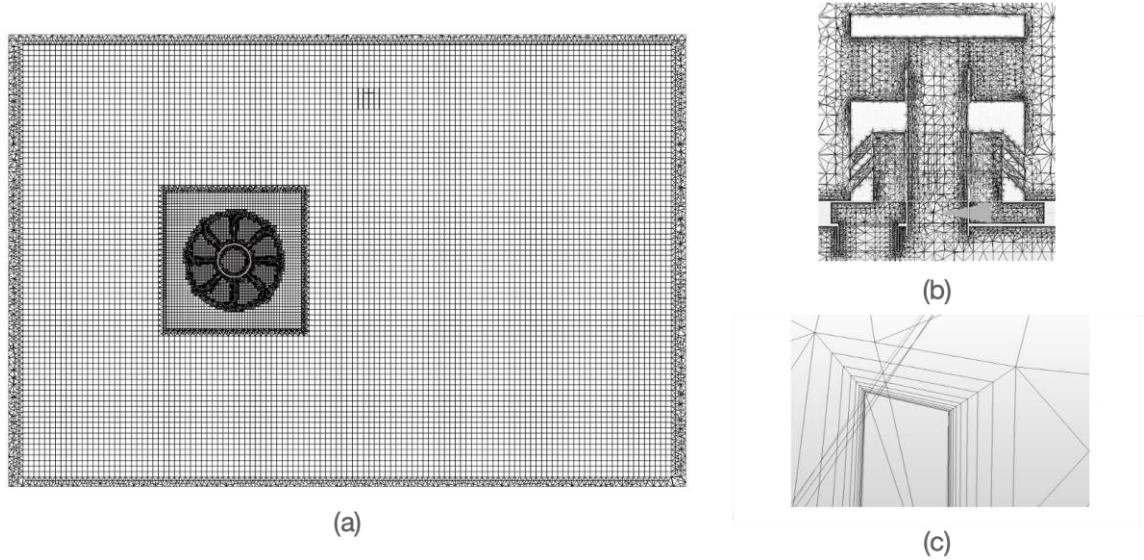


Figure 3.8. Mesh details: (a) flow domain, (b) turbine ventilator and (c) inflation layer.

To mitigate a high number of mesh cells in the simulation, multiple subdomains were built to enable mesh refinements by utilising a relatively coarse mesh further away from the geometry, whereas a finer mesh was closer to the geometry. A mesh sensitivity study was carried out to optimise the appropriate mesh size in consideration with simulation accuracy and computational cost. Four different mesh sizes (0.63, 1.12, 2.12 and 3.12 million) were applied under the same simulation conditions for the mesh sensitivity analysis. Velocity magnitudes at the centreline were measured to evaluate the mesh by comparing the root mean squared error of velocity between each mesh. The root mean squared error was calculated for 11 points from the coarse to the finest mesh, yielding 7.7%, 12.4% and 2.02%, respectively (shown in Figure 3.9).

$$\text{Root Mean Squared Error} = \sqrt{\frac{\sum_{i=1}^N \left( \frac{(x_i - x'_i)}{x_{\text{ref}}} \right)^2}{N}} \quad (3.19)$$



Where  $x_i$  and  $x'_i$  are the simulated velocity magnitudes at the measured points between two different mesh sizes, and  $x_{ref}$  represents the reference velocity magnitude. N is the number of measured points.

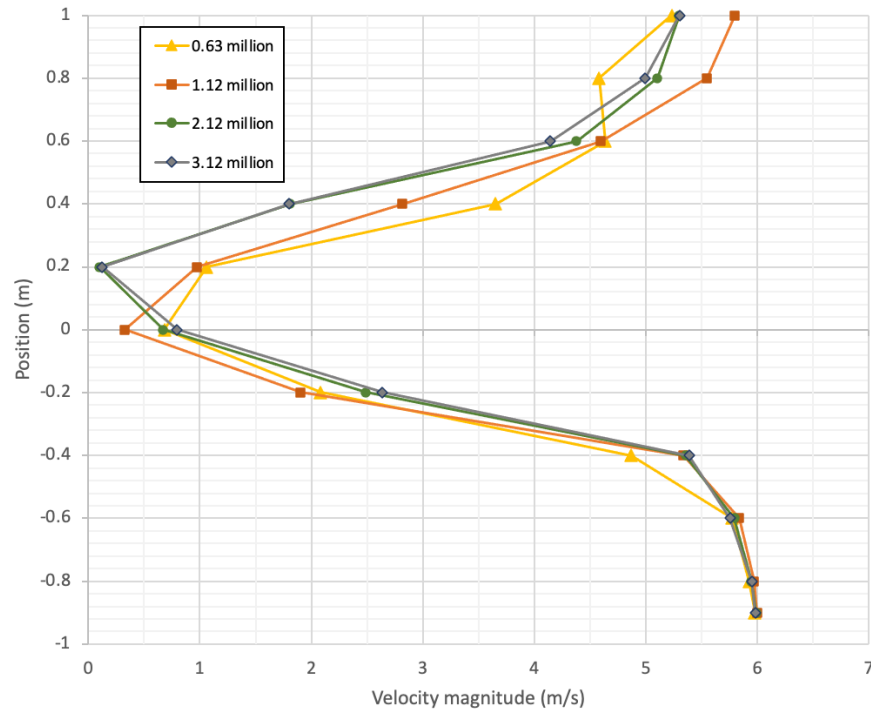


Figure 3.9. Comparison of velocity magnitudes with different mesh sizes.

The results showed that there was a slight difference between the mesh size of 2.12 and 3.12 million. However, there was a significant difference in computational resources used for the 3.21 million mesh. Hence, in this study, the 2.12 million mesh was adopted in this study. The global maximum cell size was 50m. The average skewness was 0.17435, which is within the acceptable range as per the recommendations. The overall aspect ratio was averaged 1.45. By having a high-quality mesh with an optimised number of nodes, it ensures the convergence of the

CFD simulations and the accuracy of simulation results. Figure 3.10 shows the convergence of the CFD simulation was achieved, in which residuals became stable after 5000 iterations.

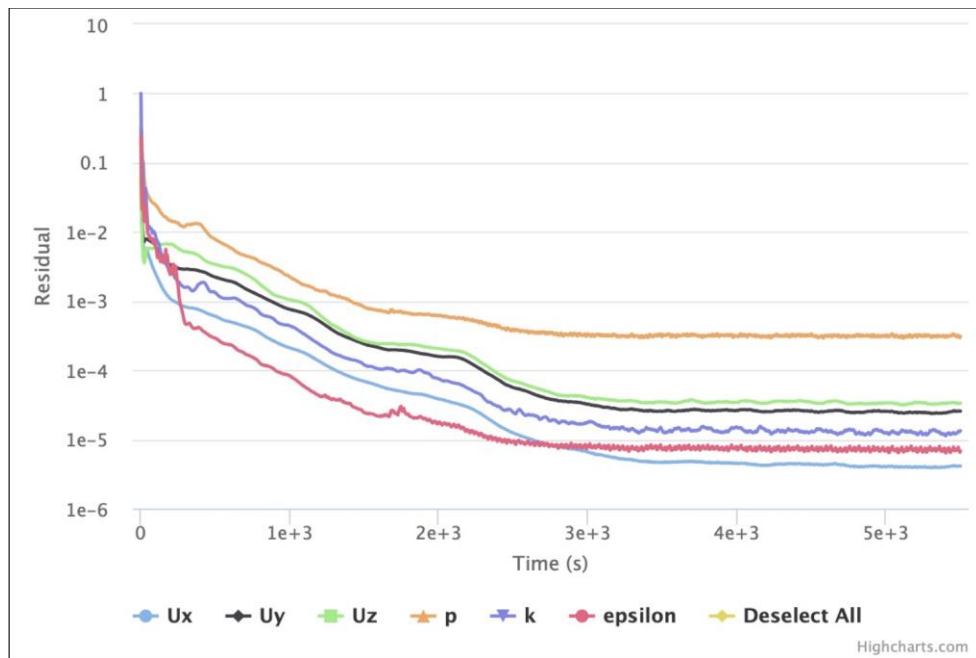


Figure 3.10. Convegence plot of the 8 blade turbine ventilator at velocity = 4 m/s.

## 4. Results and Discussion

CFD simulations were performed on the turbine ventilator model to gain a comprehensive understanding of the proposed concept of a wind driven ventilation system, specifically focusing on the performance of ventilation rates. The CFD simulation outcomes were analysed and visualised using flow patterns, illustrating the velocity and static pressure field. Subsequently, the model underwent modifications and numerical testing to investigate potential improvements in fresh air supply and stale air extraction performance. The findings from the modified model are also presented and discussed in this section. Finally, the validation of the simulation results in this study was performed by comparing them with experimental results from commercial straight vane turbine ventilators, as reported by Khan et al. (2008b) and Lien and Ahmed (2011).

### 4.1. The Initial Turbine Ventilator Model

The CFD analysis used velocity inlet settings with velocity magnitudes of 1 m/s, 2 m/s, 3 m/s, 4 m/s, 5 m/s and 6 m/s in the CFD analysis. The initial investigation involved performing CFD simulations on the proposed turbine ventilator model, featuring two different blade profiles: 2 blades (2B-TV) and 8 blades (8B-TV). This methodology facilitated the evaluation of the turbine blade profile's impact on ventilation performance, especially in relation to exhaust volume flow rate. To address SimScale's limitation, the proposed turbine ventilator model was strategically divided into two separate sections for CFD simulations. Figure 4.1

displays the CFD simulation setup, and Figure 4.2 presents the initial CFD simulation outcomes for the flow regime.

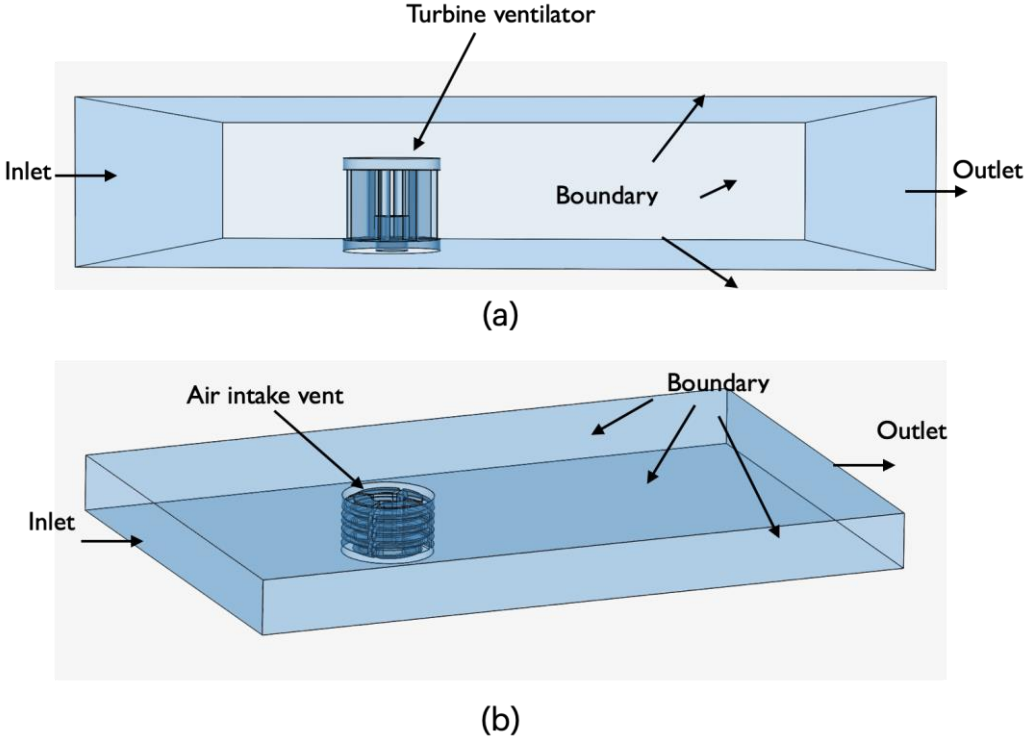


Figure 4.1. CFD simulation setup on SimScale.

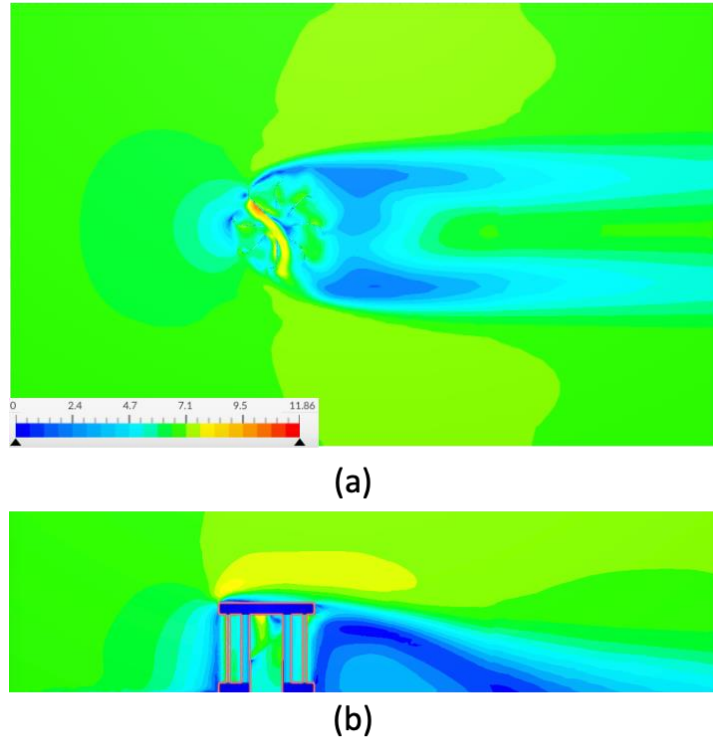


Figure 4.2 Velocity contours of initial CFD simulation results in: (a) x-y axis and (b) x-z axis.

#### 4.1.1. Air Extraction Performance

##### 4.1.1.1. 2-Blade Turbine Ventilator (2B-TV)

The CFD simulation for the 2B-TV, possessing a throat diameter of 140mm, underwent thorough analysis. Figure 4.3 exhibits the velocity contours of the 2B-TV across various velocities, captured at 100 mm above the cylindrical base of the rotor domain. Upon examining the flow pattern, a small region of recirculating flows appeared on the convex side of the blade at the top region facing the incoming flow direction. High-velocity contours were detected at the downstream convex side of the duct. These highlighted regions significantly impact pressure distributions, as demonstrated in Figure 4.5. High-pressure distribution is discernible where

recirculation transpires, whereas low-pressure distribution is prevalent in the duct subjected to high-velocity contours (see Figure 4.4).

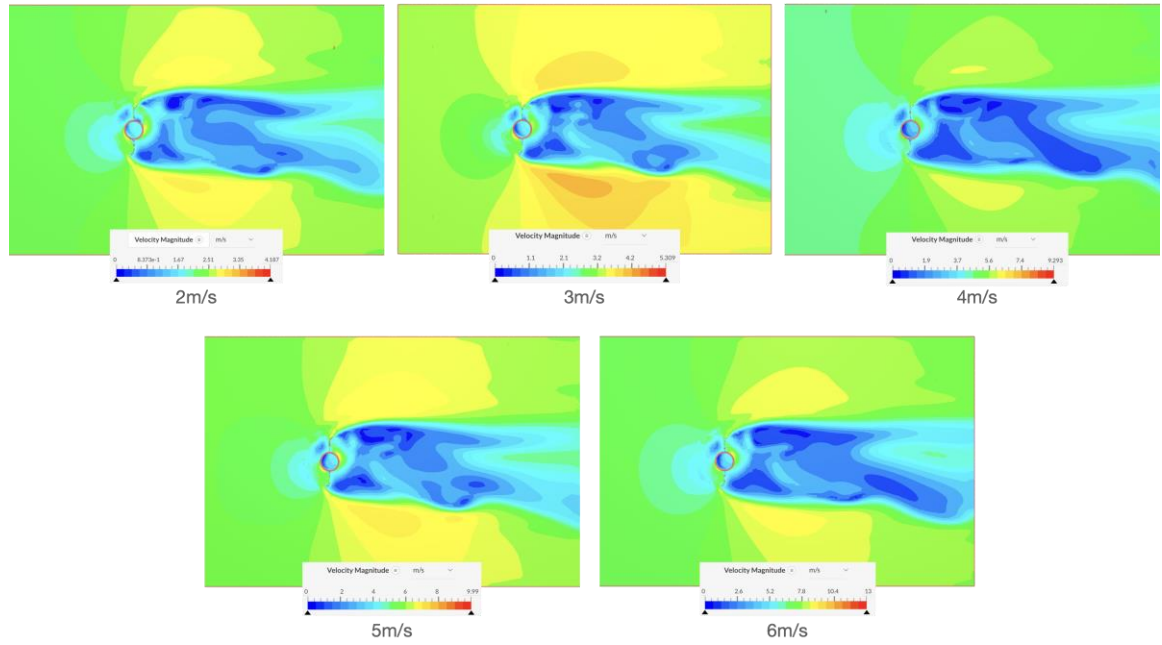


Figure 4.3. Velocity contour of the 2 blade model at different velocities.

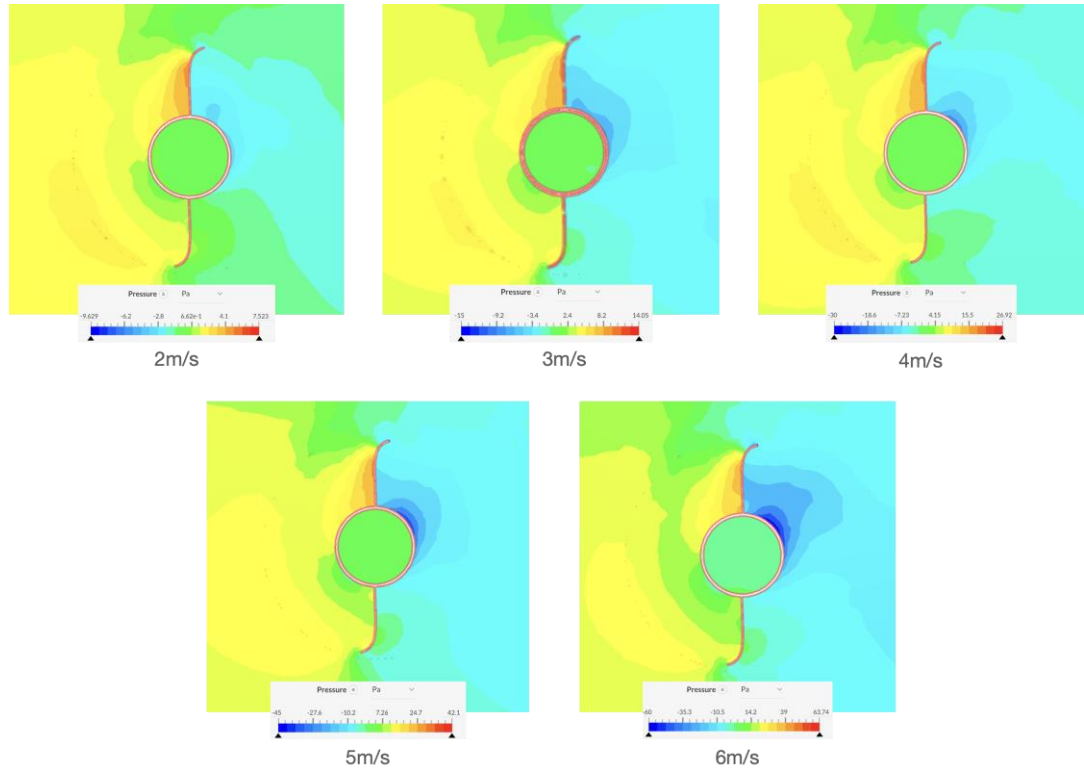


Figure 4.4. Static pressure contours of the 2-blade model at different velocity magnitudes.

Figure 4.5 indicates the correlations between high velocity and low pressure or low velocity and high pressure. The flow behaviour surrounding the turbine ventilator is illustrated in Figure 4.5a, signifying the recirculation zone of the incoming flow on the convex side of the returning blade (in the red circle), obstructing the rotation of the turbine ventilator. This suggests the highlighted region remains stagnant and induces a substantial pressure gradient on the blade convex, as portrayed in Figure 4.5b (Tian et al., 2019).

As a result, flow separation appeared around the blade edge, accompanied by low-pressure region correlated with a relatively high velocity. As flow separation occurs, the flow behaviour in the rotor's middle region exemplifies the swirling pattern of the flow, as displayed in Figure 4.6a. Swirling flows materialised near the returning

blade's inner edge, facilitating the removal and exhaustion of airflow by the turbine ventilator from the duct.

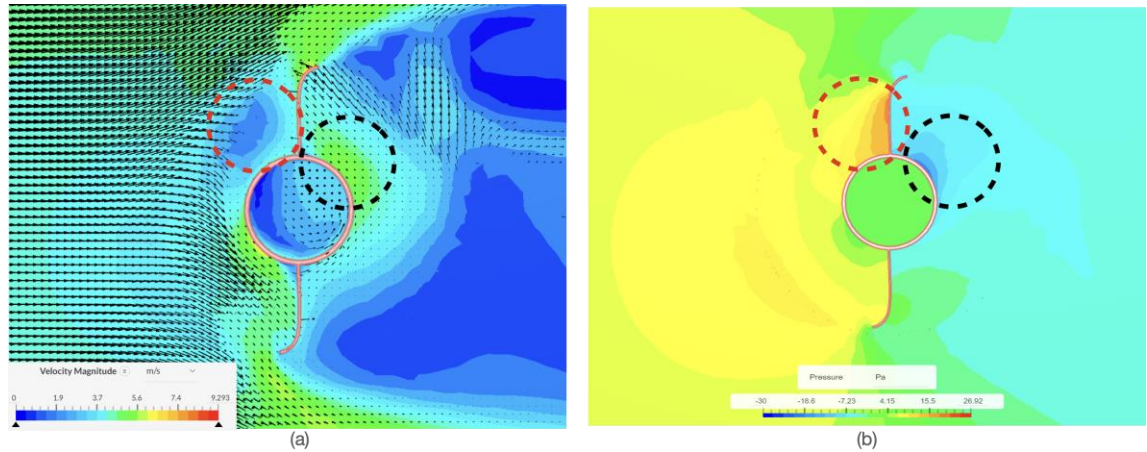


Figure 4.5. Inlet velocity of 4 m/s: (a) velocity vector and (b) pressure contour (at 100 mm above the rotor base).

In Figure 4.6a, the swirling flow's upward arrows represent the extracted exhausted air. Further observation shows that the region where the swirling pattern originates influences negative pressure generation, as shown in Figure 4.6b. Consequently, a more significant negative pressure yields superior air extraction performance for the turbine ventilator.

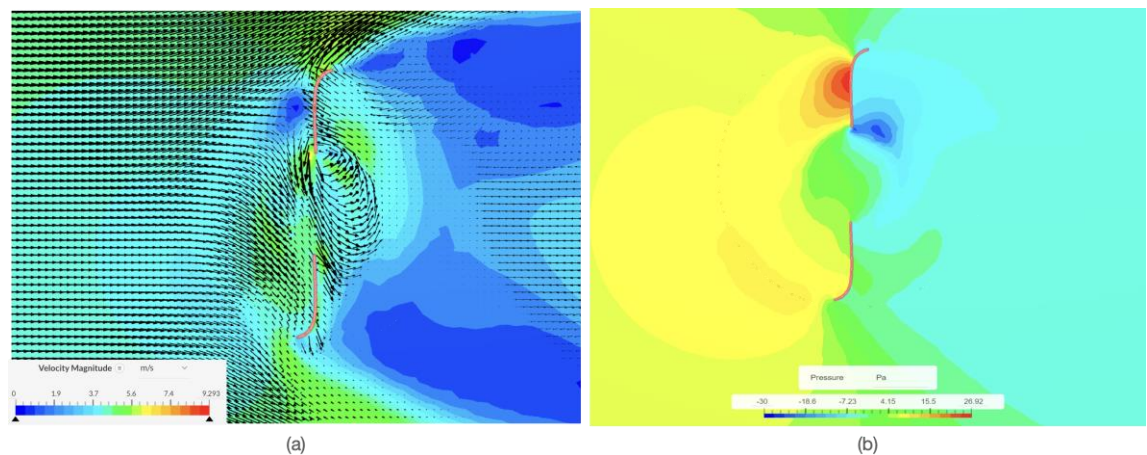




Figure 4.6. Inlet velocity of 4 m/s: (a) velocity vector and (b) pressure contour (at 160 mm above the rotor base).

To evaluate the 2B-TV model’s ventilation performance capabilities, Table 4.1 presents the CFD simulation results of exhaust flow rates at the disparate velocity magnitudes. According to the Building Regulation’s Approved Document F: Ventilation, a minimum ventilation rate of 35 l/s for the entire dwelling for air extraction is recommended, as illustrated in Appendix Table A1 (HM Government, 2022). Based on the numerical results from the CFD analysis, the mass flow rate extracted by the 2B-TV model falls short of the minimum ventilation requirement by 15.9%, considering a velocity at 6 m/s. This finding indicates that the 2B-TV model fails to satisfy the minimum ventilation rate requirement for air extraction.

Table 4.1. CFD simulation results of ventilation performance for 2B-TV model.

2B-TV Model			
Velocity (m/s)	Rotational speed (RPM)	Exhaust Volume flow rates	
		(m <sup>3</sup> /s)	(l/s)
2	48	0.0119	11.91
3	60	0.0121	12.1
4	115	0.0181	18.06
5	167	0.0241	24.08
6	216	0.0294	29.43

#### 4.1.1.2. 8-Blade Turbine Ventilator (8B-TV)

Since the 2B-TV model delivered exhaust flow rates below the minimum requirement, the 8B-TV model was developed and numerically tested to investigate its potential performance in air extraction. CFD simulations were performed with velocities ranging from 1 m/s to 6 m/s. As the incoming flow interacts with the rotating blades, a stagnation region forms, leading to a reduction in wind velocity for the rotating blade, as shown in Figure 4.7. Additionally, the development of separated flow occurs at the top of the turbine ventilator, creating a low-pressure area. The incoming flows began entering the inner domain of the turbine ventilator from the top left corner and exited through the bottom, causing the inner flows to swirl within the turbine ventilator's interior (see Figure 4.8). This behaviour of the inner flows becomes a contributing factor to the turbine rotation (Tian et al., 2019).

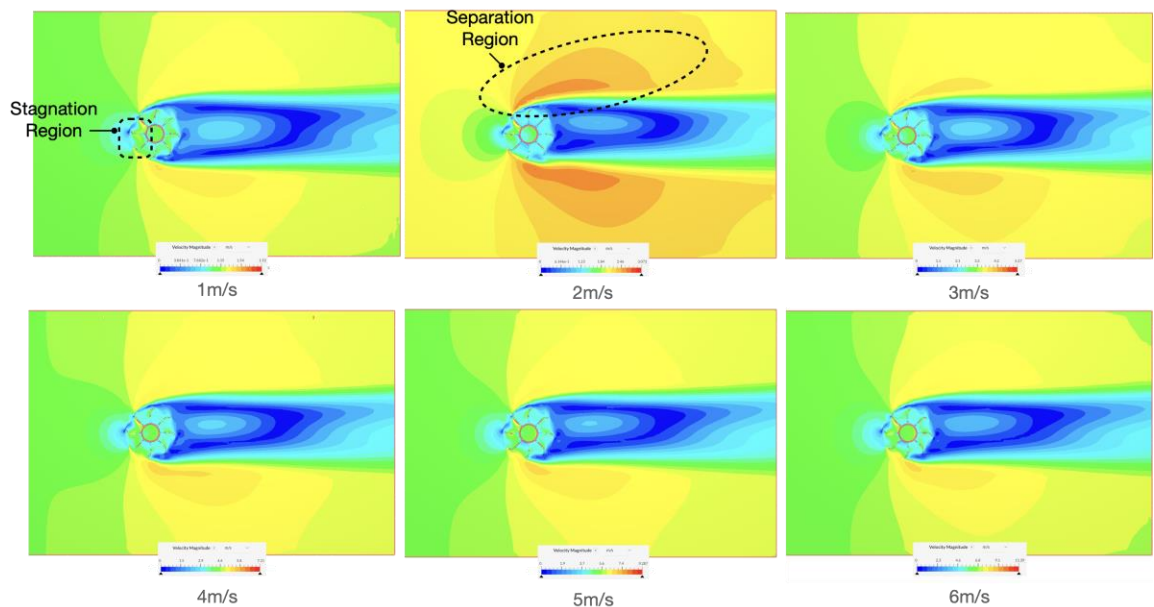


Figure 4.7. Velocity contours of the 8B-TV model at 100mm above the rotor base.

The interaction of the inner flows within the rotor led to the formation of a vortex at the top right above the duct, as shown in Figure 4.8b, causing a reduction in pressure around its area. The effect of stagnation region (encircled black in Figure 4.8a) resulted in significant positive pressure at the tip of the returning blade zone (encircled red in Figure 4.9a). With an increase in wind speed of the inner flow passing through the rotor, the development of negative pressure was influenced by the inner flow velocity as shown in Figure 4.9b.

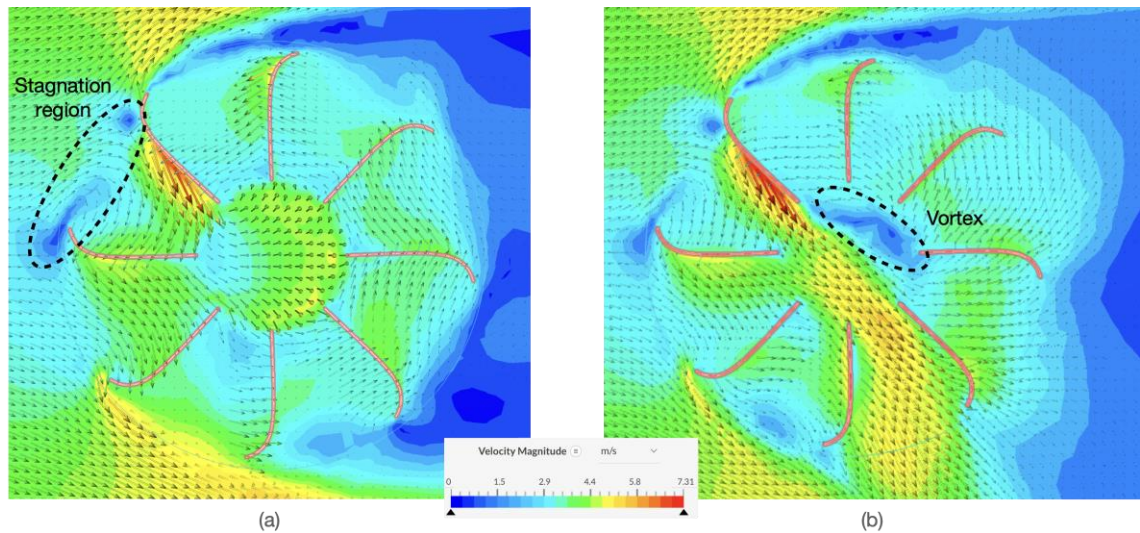


Figure 4.8. Contours and vector of velocity for the 8B-TV model at velocity of 4 m/s: (a) at 160mm and (b) at 300 mm above the cylindrical base.

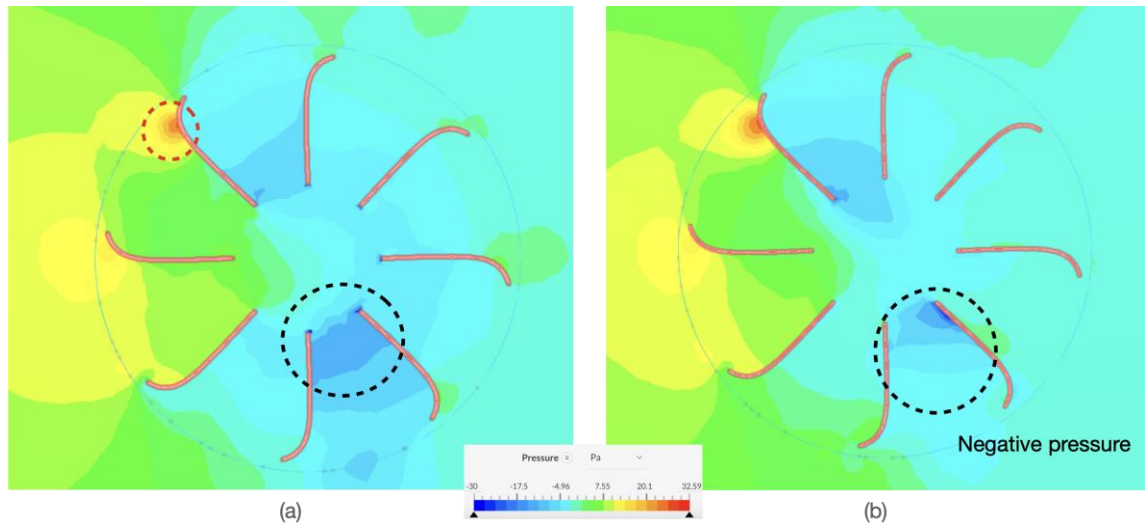


Figure 4.9. Contours of pressure for the 8B-TV model at velocity of 4 m/s: (a) at 160mm and (b) at 300 mm above the cylindrical base.

In Figure 4.10 shows that the extracted airflow induced by the turbine ventilator started covering an area to the right hand of the turbine ventilator as wind velocities increased. This created vortices in the area, leading to negative pressure on the suction effects of airflow from the duct (see Figure 4.11). It is observed that the 8-blade profile had a great impact on the pattern of swirling flows, inducing greater extraction flow rates. Moreover, the wake behind the turbine ventilator increased the swirling flows within the rotor, resulting in enhanced suction effects. Table 4.2 presents a summary of the CFD results for the 8B-TV model's air extraction performance. With a minimum dwelling extraction ventilation rate requirement of 35 l/s, the 8B-TV model could achieve the minimum requirement at a velocity of 3 m/s.

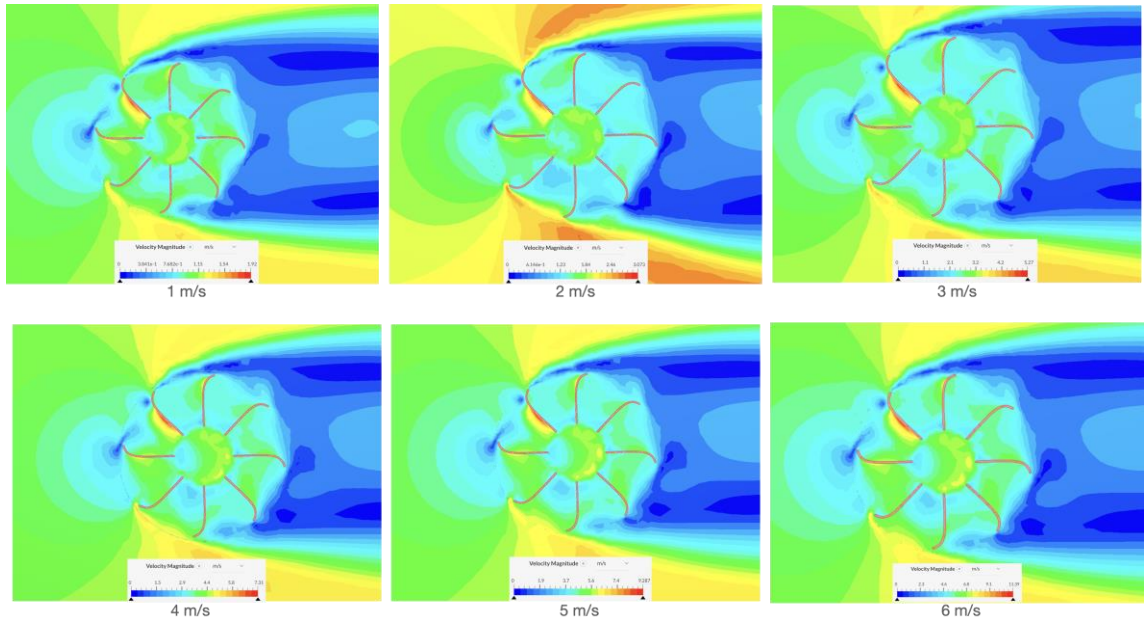


Figure 4.10. Contours of velocity for the 8B-TV model at 160 mm above the rotor base.

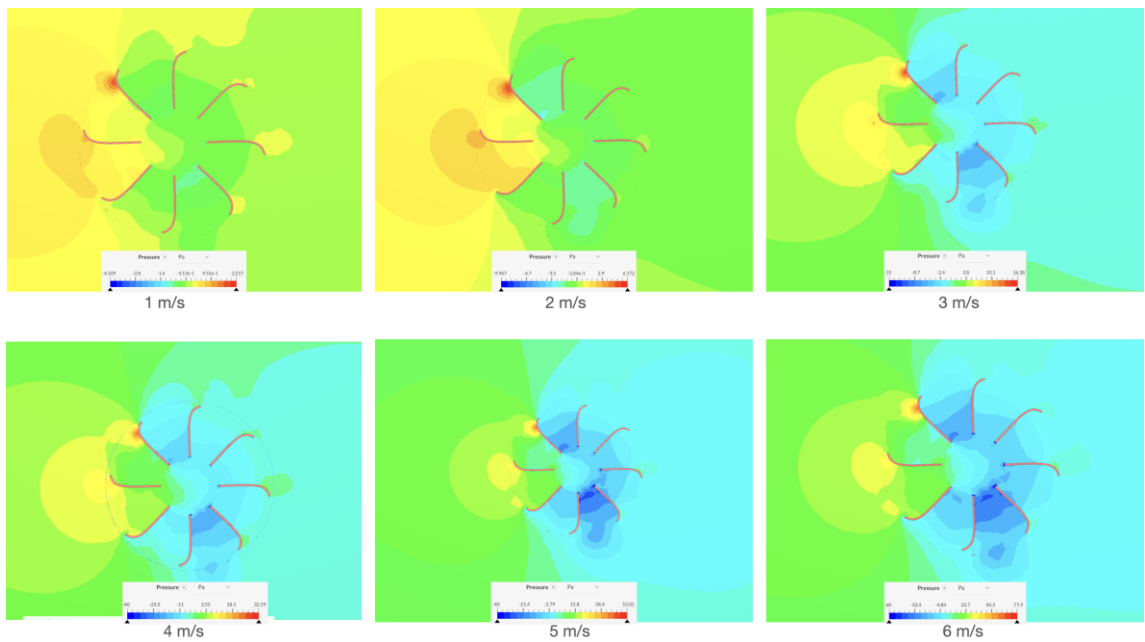


Figure 4.11. Static pressure constours of the 8B-TV model at 100mm above the rotor base.

Table 4.2. CFD simulation results of ventilation performance for 8B-TV model.

8B-TV model				
Velocity	Exhaust Volume flow rates		Static pressure	
(m/s)	(m <sup>3</sup> /s)	(l/s)	(Pa)	(Pa.m <sup>2</sup> )
1	0.01316	13.16	-0.64	-0.0077
2	0.01900	19	-1.41	-0.0154
3	0.03559	35.59	-4.38	-0.0514
4	0.05350	53.5	-9.14	-0.1137
5	0.07041	70.41	-15.42	-0.1952
6	0.08752	87.52	-23.55	-0.3003

#### 4.1.2. Air intake vent (AIV)

The performance of the fresh air intake vent (AIV) model was assessed through CFD simulations, focusing on the induced flow rate entering the AIV model. The simulations were conducted under steady-state conditions and with a wind flow inlet angle of 0°. The AIV model's CFD result at a velocity magnitude of 6 m/s is presented.

Figure 4.12 illustrates the velocity contours of the AIV, captured at different heights above the cylindrical base (50 mm, 100 mm, and 150mm). The contours reveal a stagnation point flow at the windward side of the AIV, accompanied by flow separation on each side of structure.

In Figure 4.13a, the velocity field distribution at the bottom of the AIV supply channels is depicted, demonstrating the passage of induced flow through the windward side opening. The velocity vectors represent the flow patterns of the oncoming wind captured and induced by the AIV, with airflow leaving through other channels (Figure 4.13b). As shown in Figure 4.14, a negative pressure region forms at the top, bottom, and leeward sides of the AIV model due to flow separation, which results in pressure reduction.

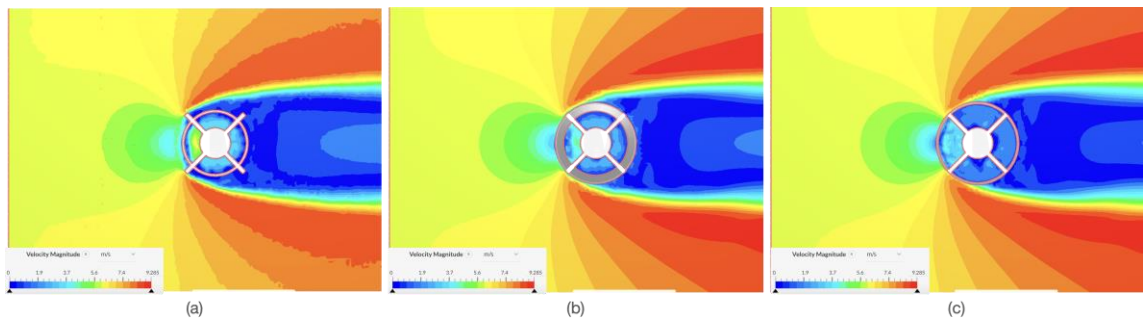


Figure 4.12. Contours of velocity for air intake vent at velocity of 6 m/s: (a) at 50 mm, (b) at 100 mm and (c) at 150 mm.

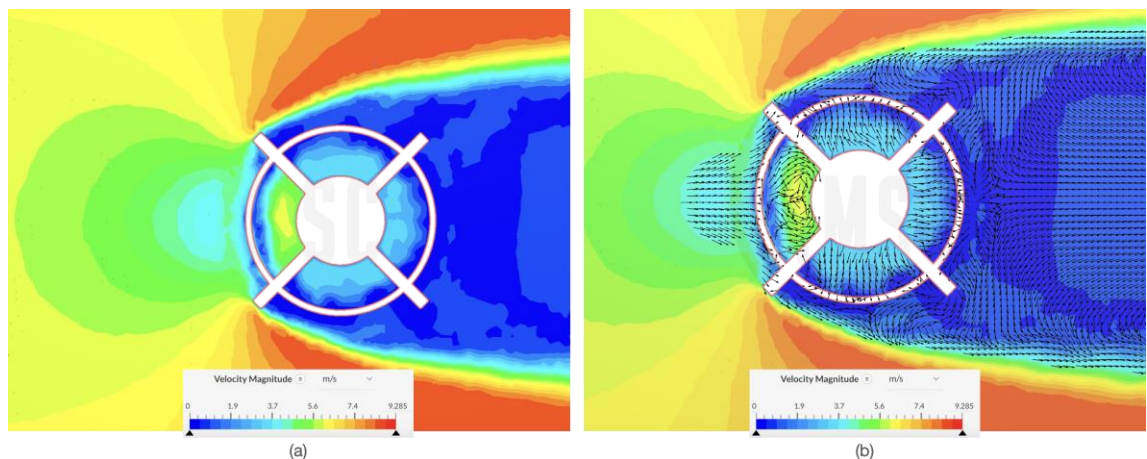


Figure 4.13. Distribution of wind velocity at the bottom of the AIV supply channel: (a) velocity contour and (b) velocity vector.

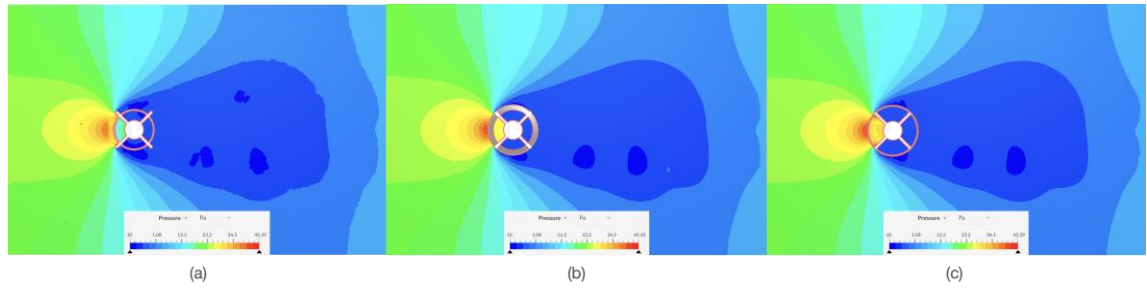


Figure 4.14. Contours of pressure for air intake vent at velocity of 6 m/s: (a) at 50 mm, (b) at 100 mm and (c) at 150 mm.

Figure 4.15 displays the cross-sectional plane velocity and pressure contours of the AIV model, highlighting the correlation between these variables. The velocity contours in Figure 4.15a show recirculation zones formed on the outer wall at the lower edge of the louver bend (encircled in red) after airflow entry through the inlet opening. This flow separation, caused by sudden flow direction changes at sharp corners at the bend, adversely affects the supply airflow rate performance (Alsailani et al., 2021). As the flow progresses towards the rear wall, a larger recirculation zone and flow separation are accelerated. The pressure contours of the cross-sectional plane in the supply channel (See Figure 4.15b) indicate a substantial pressure gradient near the upper wall of the bend and the louver. This high-pressure area contributes airflow loss, decreasing the mass flow rate within the air supply channel.

The CFD simulation conducted at a velocity of 6 m/s yielded an average pressure of 27.26 Pa for the AIV supply channel, with an induced air supply rate of 38.25 l/s. The mass flow rate results of the AIV model at different velocities are detailed in Appendix Table A3. Given the ventilation performance based on numerical results, potential



improvements can be achieved by in minimising in flow losses via modifications to the AIV's design features.

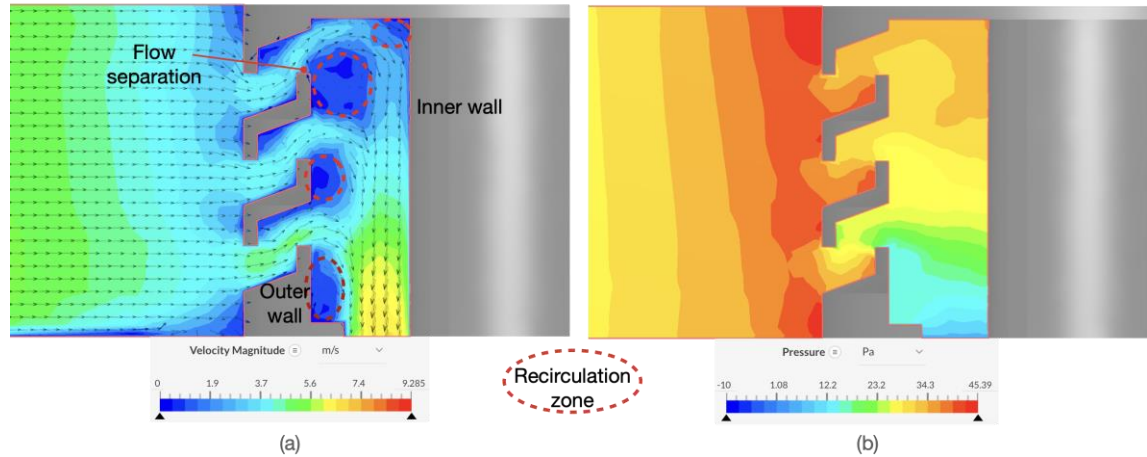


Figure 4.15. Cross-sectional plane of the AIV model at velocity of 6 m/s: (a) velocity and (b) pressure contour.

#### 4.1.3. Performance Comparison and Analysis of Proposed Turbine Ventilator Design

To investigate the potential of the proposed turbine ventilator design, CFD simulations for the 2B-TV and 8B-TV models were conducted to analyse the influence of the blade profiles their performance in home ventilation systems. Figure 4.16 shows a comparison of the numerical results for ventilation performance between the 2B-TV and 8B-TV models, with exhaust mass flow rates plotted against wind speed.

The 8B-TV model greatly outperformed the 2B-TV by 66% for wind speeds above 2 m/s. At a wind speed of 6 m/s, the 2B-TV model failed to achieve the benchmark ventilation rate of 35 l/s for dwellings. On the contrary, the 8B-TV satisfied the

minimum ventilation rate at the wind speed of 3 m/s, with an extracted volume flow rate of 35.59 l/s. The comparison highlights the superior exhaust ventilation flow rates performance of the 8B-TV model.

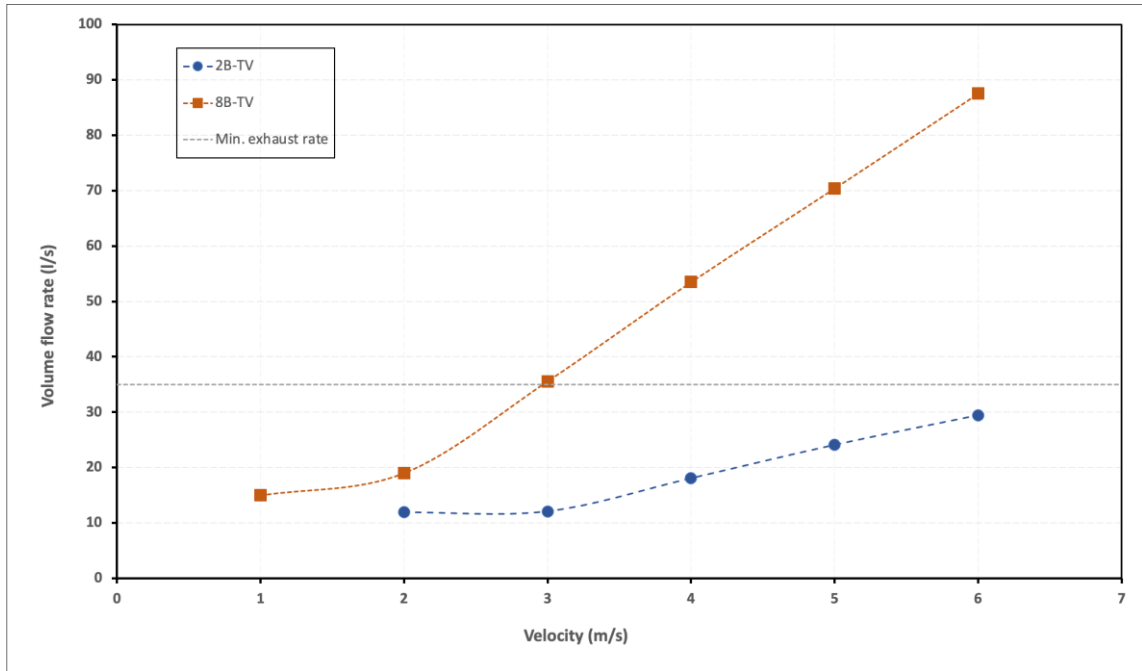


Figure 4.16. Comparison of the ventilation performance of 2B-TV and 8B-TV.

To validate the CFD results of the 8B-TV model, the results of this study were compared with experimental and numerical results from Khan et al. (2008b) and Ghanegaonkar et al. (2018). The comparisons included 300 mm and 250 mm straight vane turbine ventilators from Khan et al. (2008b) and a 600 mm curved turbine ventilator from Ghanegaonkar et al. (2018). In Figure 4.17 demonstrates that the present study's results align with those of the 250 mm straight vane turbine ventilator by Khan et al. (2008b). Despite the difference in throat diameter, the 8B-TV model with a 140 mm throat diameter induced airflow comparable to the Khan's

250mm turbine ventilator. The overall trend in ventilation performance of the 8B-TV model was consistent with results of other studies.

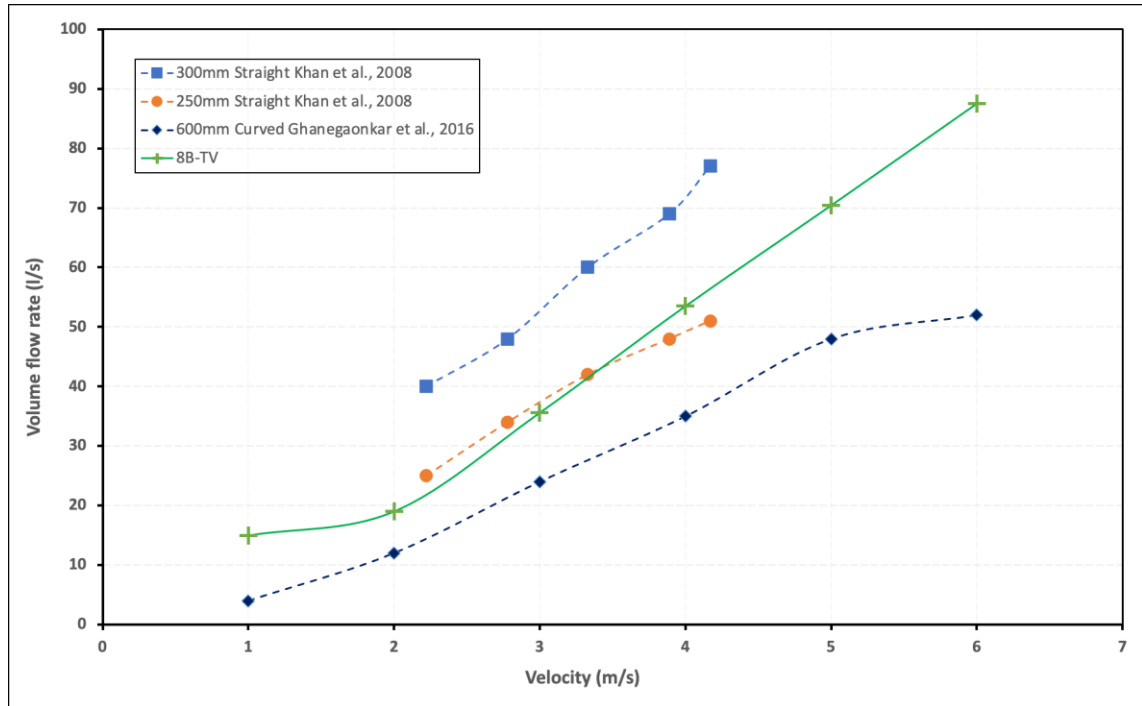


Figure 4.17. Comparison of the ventilation performance of the turbine ventilators with other studies.

Figure 4.18 shows the AIV model's simulation results for volume flow rates induced at wind velocities ranging from 2 m/s to 6 m/s. The figure illustrates a linear relationship between increasing induced flow rates and increasing wind velocities. Considering the whole dwelling ventilation rate for air supply suggested by the Building Regulation, the AIV model's induced flow rates met the minimum requirement for 1, 2, 3 and 4 bedrooms at wind speeds of 3.8 m/s, 5 m/s, 5.5 m/s and 6 m/s, respectively. However, the 5-bedroom requirement was not met due to the AIV's maximum ventilation rate of 38.25 l/s at 6 m/s wind speed.

Although the minimum requirement could be met at a wind speed above 7 m/s, this is not in line with the proposed turbine ventilator’s intended functionality at low wind speeds between 1 and 6 m/s. To enhance the AIV model’s efficiency at low wind speeds, further modifications were made. Figure 4.19 and 4.20 display performance curves, illustrating the relationship between ventilation flow rate and pressure produced by the proposed turbine ventilator. The figures indicate that pressure drop significantly impacts the 8B-TV model’s ventilation performance, with a larger pressure drop resulting in increased extracted airflow.

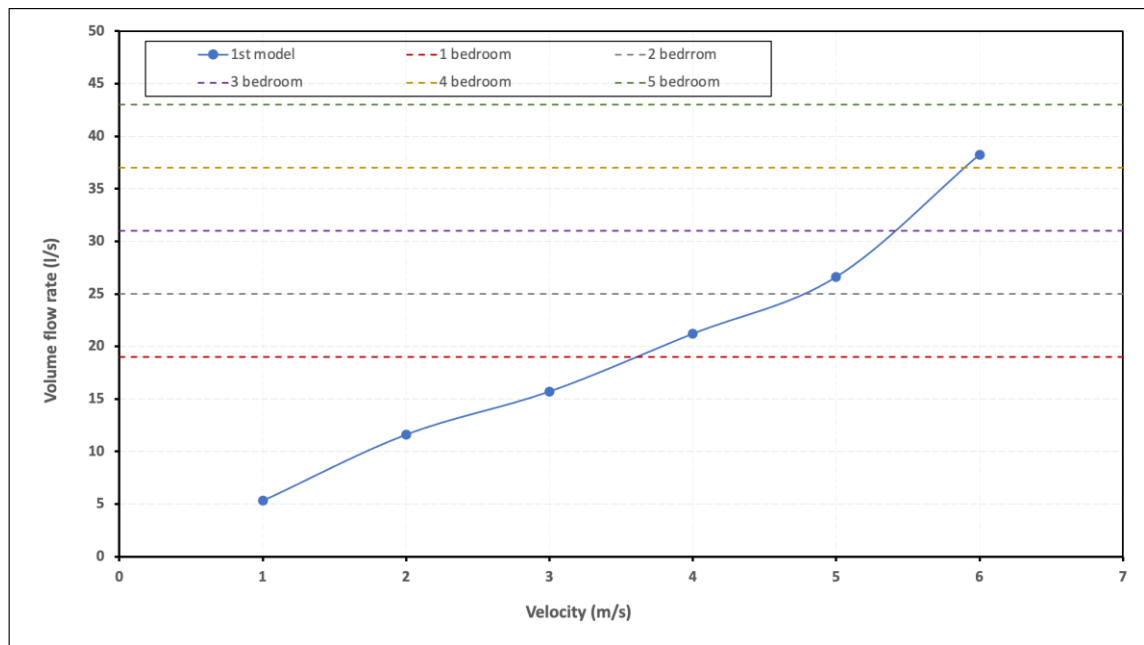


Figure 4.18. Volume flow rates induced by the AIV model.

Similarly, the mass flow rate induced by the AIV is substantially influenced by pressure, as shown in Figure 4.20. The correlation between the airflow and pressure can be simplified: as static pressure increases, the induced airflow volume decreases (Alsailani et al., 2021).

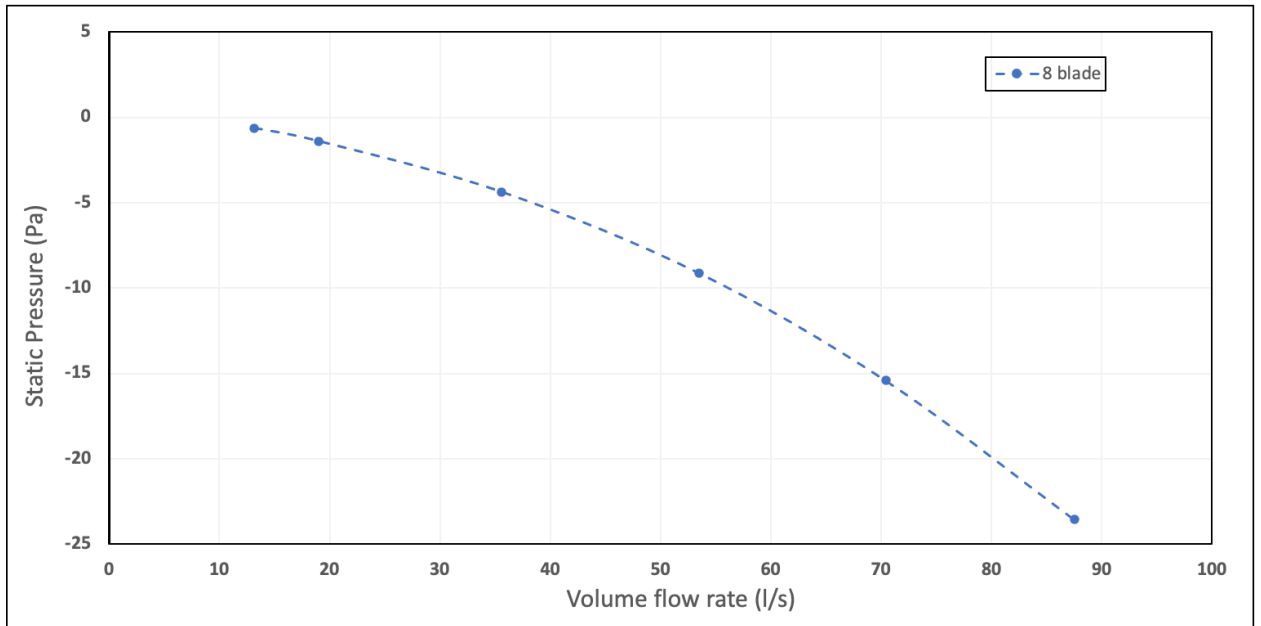


Figure 4.19. Performance curve of the 8B-TV model.

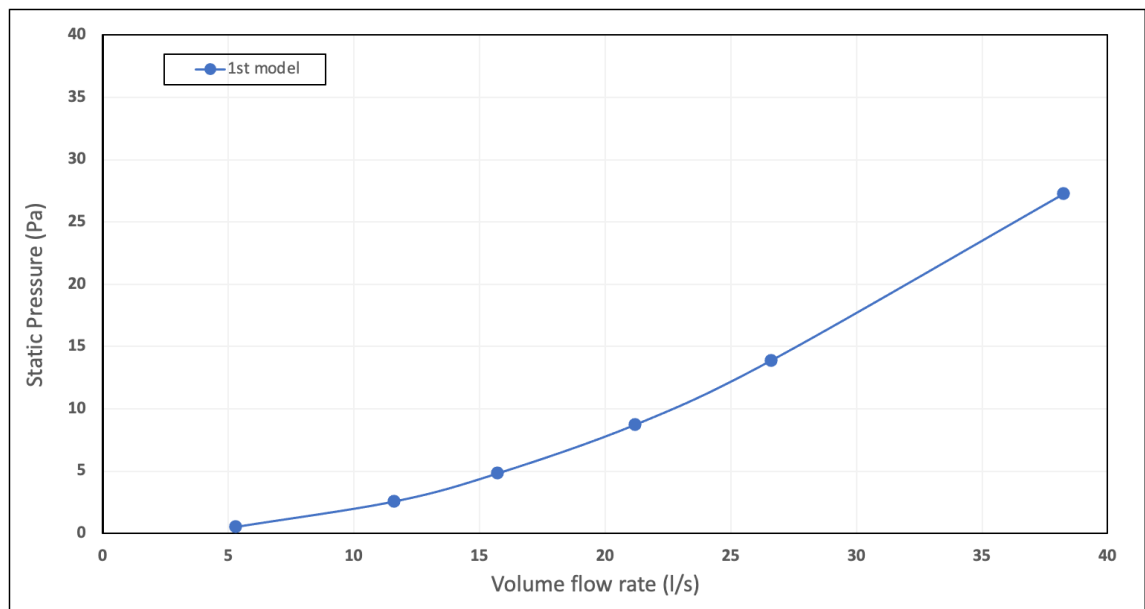


Figure 4.20. Performance curve of the AIV model.

#### 4.2. Modifications of Turbine Ventilator Model

In the preceding section, the proposed turbine ventilator design was evaluated through numerical testing and analysis. Performance predictions were made based

on CFD simulations, with results compared to data from other studies and the Building Regulation's minimum ventilation rate requirements. The assessment of the turbine ventilator's performance revealed an exhaust volume flow rate of 87.52 l/s at a wind speed of 6 m/s and a volume flow rate of 38.35 l/s for the air supply. The minimum ventilation rate for air extraction was satisfied when the wind speed exceeded 3 m/s. However, the supply flow rate induced by the turbine ventilator did not meet the minimum requirement for whole dwelling ventilation in a 5-bedroom configuration.

To further optimise turbine ventilator's performance, several design modifications were considered and subsequently subjected to numerical testing. These modifications included reducing the blade height from 300 mm to 150 mm, increasing a blade number to 10, and making alternations and additions to the AIV features. The results for the refined model are presented and discussed in the following sections.

#### 4.2.1. Blade Height Reduction

Blade height is a critical parameter that significantly impacts a turbine ventilator's performance. Khan et al. (2008b) found that increasing the height of blades by 50% could improve mass flow rates by 13.5%. This study considered a decrease in blade height to explore the differences in turbine blade performance, aiming for greater efficiency at lower wind speeds.

Figure 4.21 shows the dimensions of the modified turbine blades and a three-dimensional CAD model for CFD simulations. The blade height was reduced by 50%

to 150 mm, and the duct was extended 75 mm from the base. The computational domain setup show in Figure 3.6 was employed for CFD simulation of the modified 10-blade turbine ventilator (10B-TV). The same boundary condition settings for the 8B-TV were adopted in this CFD analysis. Autodesk CFD was used to performed simulations to investigate the effects of blade height on modified 10B-TV's ventilation performance.

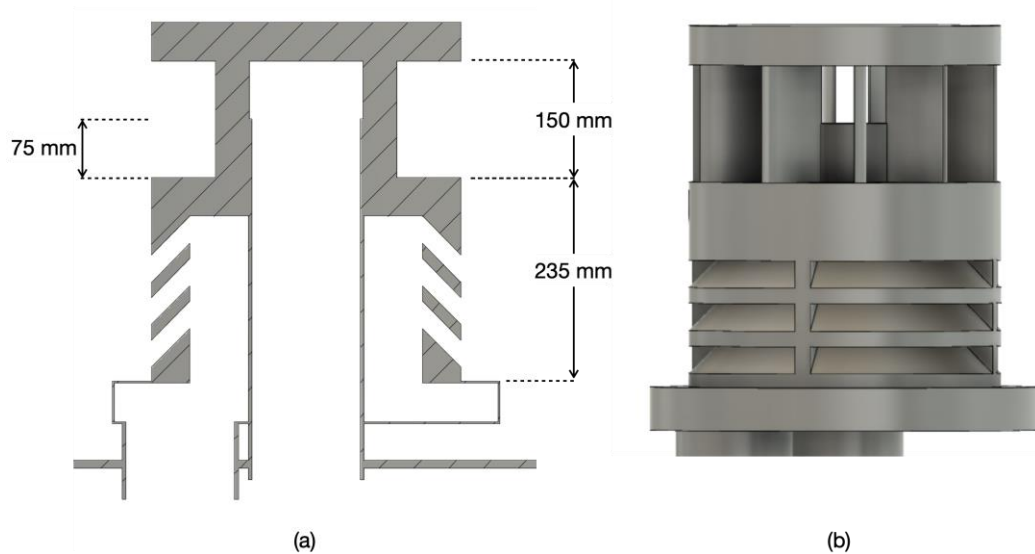


Figure 4.21. The modified turbine blades (a) schematic view and (b) 3D CAD model.

In Figure 4.22, the formation of vortices occurs in the it demonstrates the rotor's mid-region, corresponding to increasing wind speeds. With the incoming flow interacting on the windward side of the modified 10B-TV, a stagnation point formed, where the local velocity equivalent to zero. As a result, a large positive pressure was produced on the convex side of the returning blades (see Figure 4.23). This stagnation point flow extended towards along the rotating blades, leading to flow separation upstream of the rotor domain.

Similar flow characteristics were observed in the 8B-TV; however, in this case, the flow began entering the inner domain from downstream as more inner flow swirled within the rotor, causing the turbine to rotate counterclockwise. As wind speeds increased, the flow swirled faster, forming vortices in the rotor domain's centre. A negative pressure developed inside the rotor, leading to an increase in the exhaust flow rate. This indicates the correlation between airflow and pressure in determining the exhaust mass flow rate.

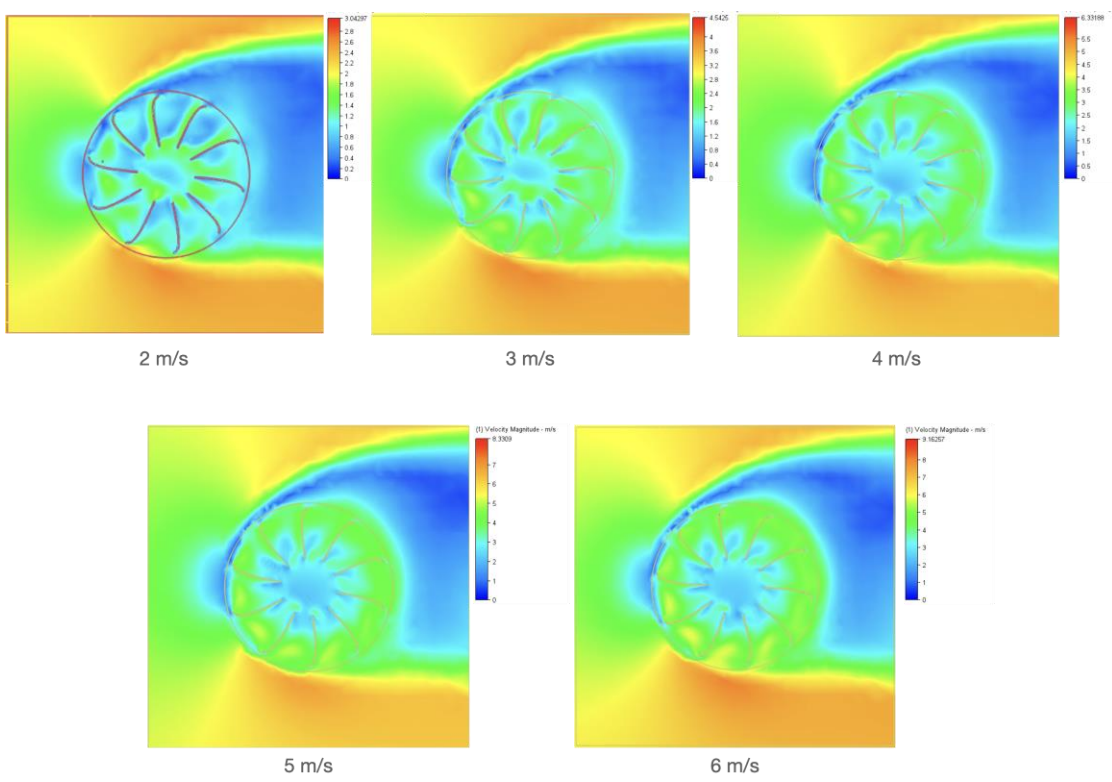


Figure 4.22. Contours of velocity of the modified 10B-TV at various wind speed.



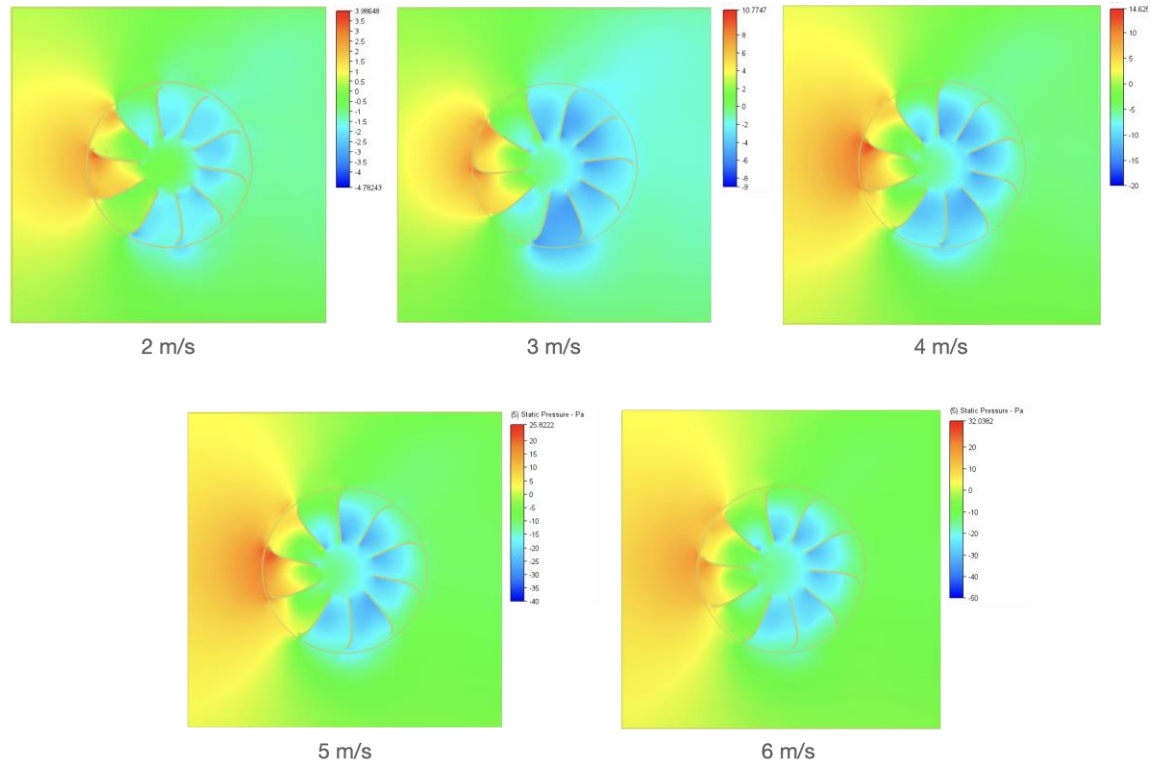


Figure 4.23. Contours of pressure of the modified 10B-TV at various wind speed.

Figure 4.24a illustrates the velocity vector, indicating the flow direction within the rotor region at a wind speed of 6 m/s. A draft was created at the centre due to the increasing swirling flow inside the rotor. In Figure 4.24b, the pressure distribution was determined by the flow velocity, with a large positive pressure forming in the low-velocity area. Conversely, the low-pressure area occurred in the high-velocity region. Consequently, an exhaust flow rate of 45.18 l/s at a 6 m/s wind speed was obtained. The modified 10B-TV ventilation performance results are provided in Appendix Table A6. The exhaust flow rates from the CFD simulations were plotted with respect to various velocities (see Figure 4.25).

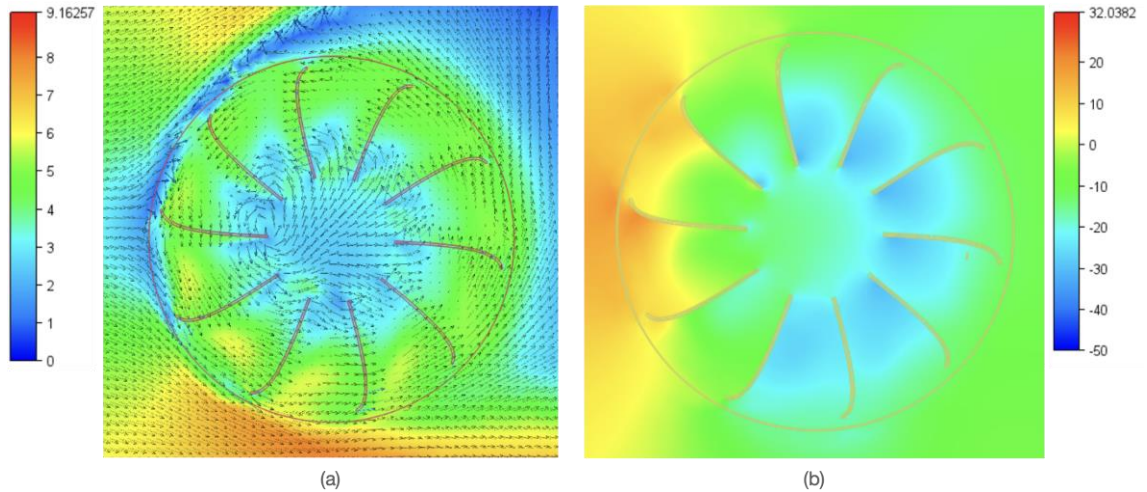


Figure 4.24. Ventilation performance of modified 10B-TV at a velocity of 6m/s: (a) Velocity vector and (b) pressure contours

The modified 10B-TV's performance exceeded the 2B-TV by 32% to 45% after 3 m/s. However, the modified 10B-TV's results were inconsistent with the 8B-TV's CFD results, with nearly a 50% difference in air extraction performance. This difference can be attributed to the 50% reduction in blade height. Although the modified 10B-TV met the minimum ventilation rate at 5 m/s, the modifications significantly reduced the volume flow rate.

When compared to the numerical and experimental results of other studies, the modified 10B-TV model underperformed, as shown in Figure 4.26. In addition, a noticeable similarity in performance was observed between the modified 10B-TV and Ghanegaonkar et al. (2018)'s 600mm model. The modified 10B-TV demonstrated superior performance at lower wind speeds, specifically 2 m/s; however, beyond a certain speed, its volume flow rate decreased.

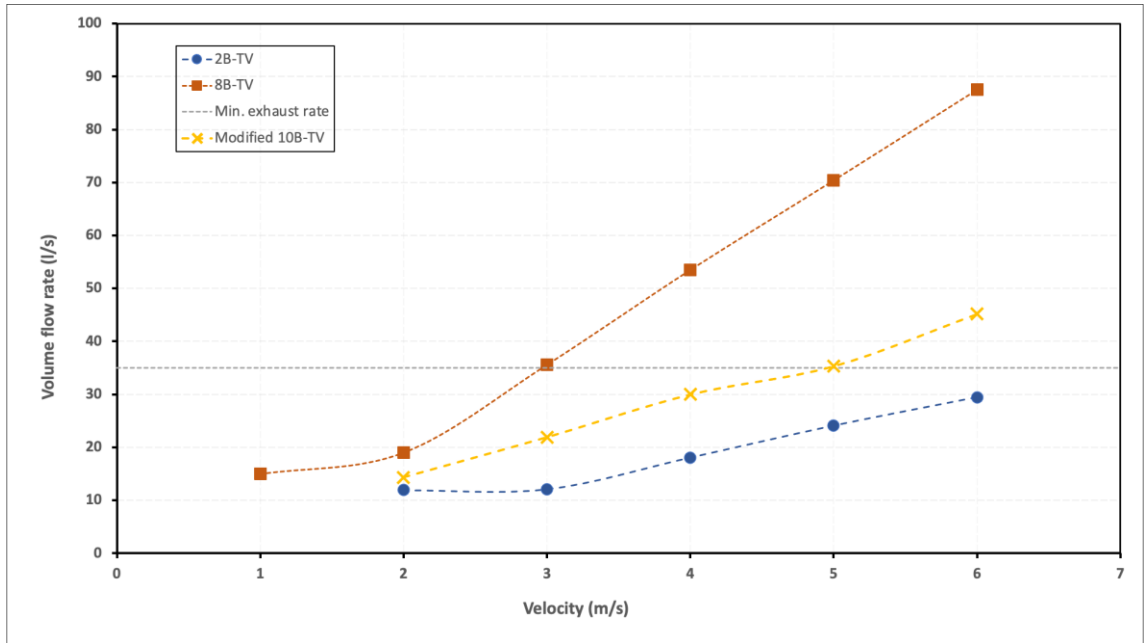


Figure 4.25. Comparison of the modified 10B-TV ventilation performance with the 8B-TV model.

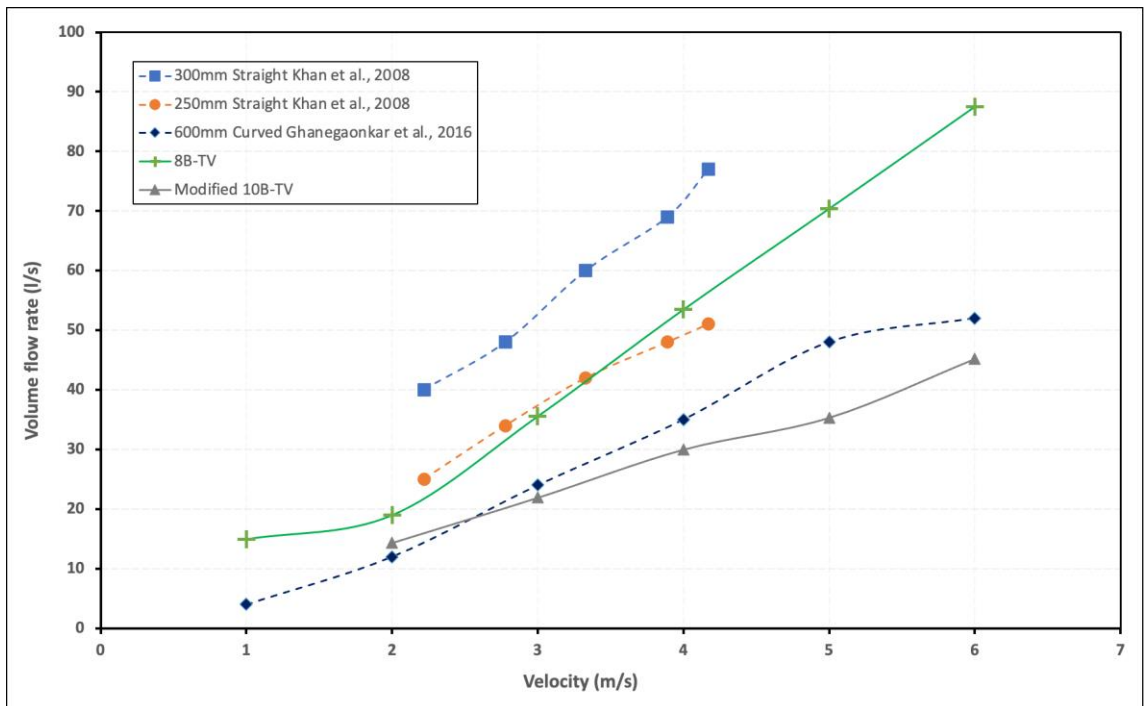


Figure 4.26. Comparison of the modified 10B-TV ventilation performance with other studies.

#### 4.2.2. Modifications of Design Features of Air Intake Vent

Upon analysing the CFD results of the original AIV model, it was found that the development of recirculation zones resulted from separated flow formed near corners at the bend, leading to increased flow losses and pressure drop. To minimise the pressure drop in the AIV, alterations to the AIV profile were considered. As flow separation and recirculation zones occurred at sharp corners of the bend, the 90° bends of the louvers at inlet opening were simplified (see Figure 4.27a). Alsailani et al. (2021) found that adding guide vanes in the bends substantially improved airflow uniformity within the supply channel, leading to an increase in airflow rate up to 29%. Consequently, in Figure 4.27b, the modified AIV2 model was modified by rounding sharp corners at the bend and adding guide vanes at the end of the inlet opening.

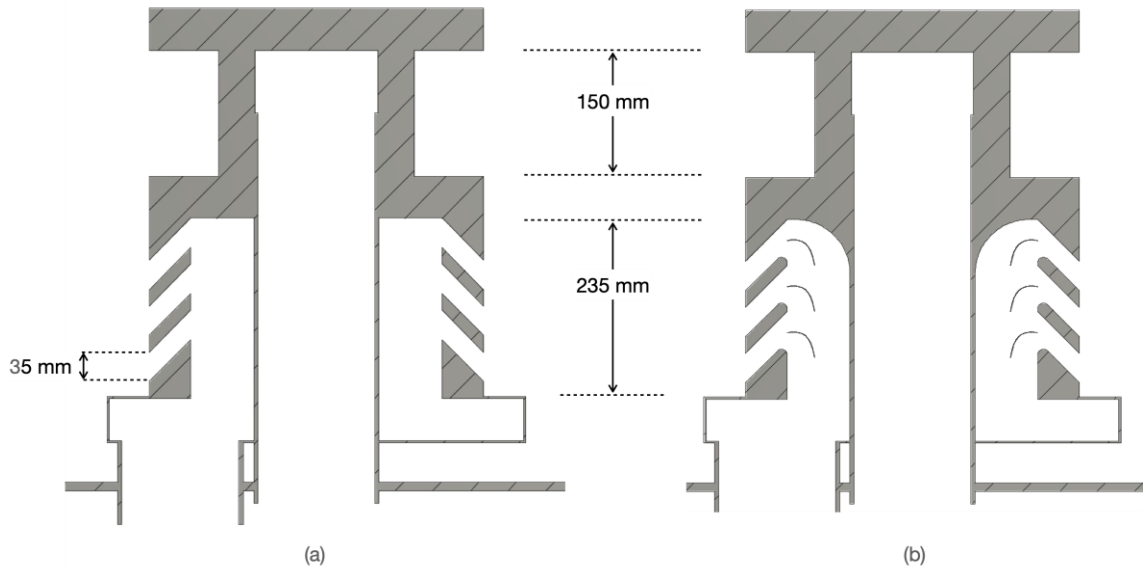


Figure 4.27. Schematic of (a) Modified AIV1 and (b) Modified AIV2.

To evaluate the impact of these modified models on ventilation performance, CFD simulations were undertaken using SimScale. The CFD results of the modified AIV1

and AIV2 at a velocity of 6 m/s are presented. Figure 4.28a shows a reduction in the size of recirculation zones (encircled in red) compared to larger recirculation zones of the AIV in Figure 4.15. This allowed for an increase in airflow to travel inside the supply channel, reducing pressure drop in the supply channel, as shown in Figure 4.28b. The supply flow rate of air induced by the modified AIV1 was determined at 40.83 l/s at a wind speed of 6 m/s.

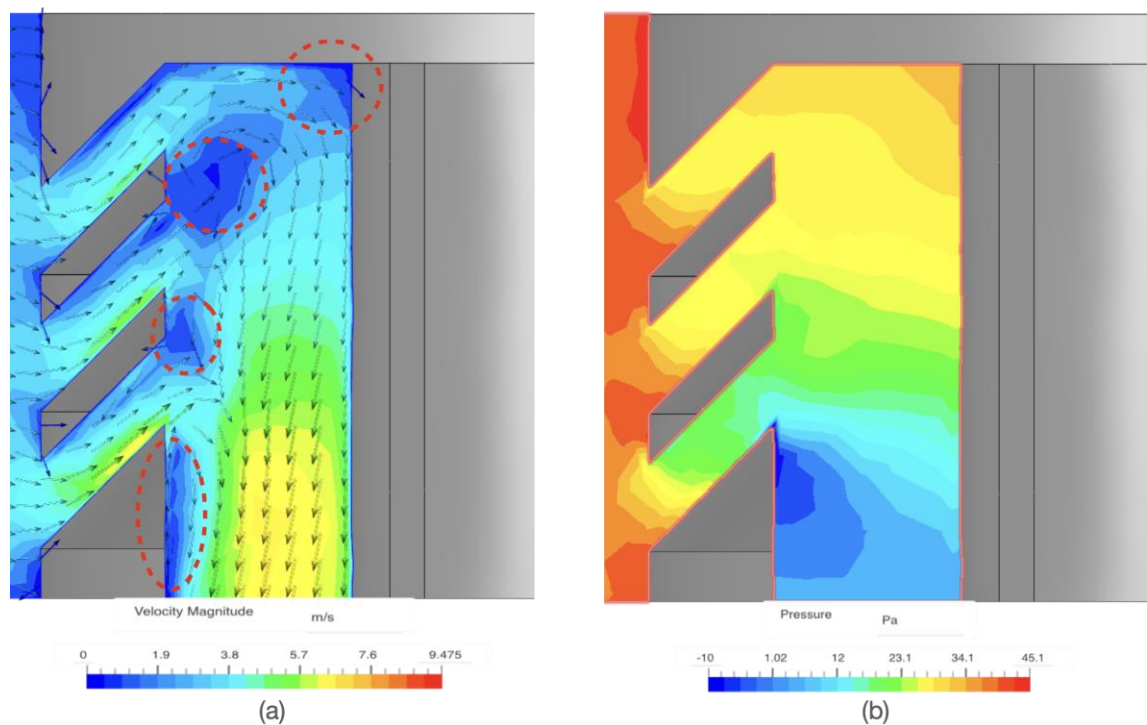


Figure 4.28. Contours of (a) velocity and (b) pressure of the modified AIV1 at velocity of 6 m/s.

Moreover, the outcomes presented by the modified AIV2, as shown in Figure 4.29, indicate a less substantial reduction in recirculation zones formation than initially anticipated when compared to the original AIV. Nevertheless, an increase in airflow at the upper right corner can be observed, which can be due to the combined effect

of the rounded corner and the guide vane directing the flow at the separation point to follow a consistent direction. The maximum velocity recorded in the channel reached 8.37 m/s, surpassing the modified AIV1's maximum velocity of 6.81 m/s. Consequently, the modified AIV2 design led to a notable change in pressure drop, as shown in Figure 4.29b. This finding emphasises the inverse relationship between air flow and pressure, with airflow increasing as pressure decreases. The supply airflow rate was determined to be 48.11 l/s in volume. Owing to the influence of modified AIV1 and AIV2 models, the ventilation performance of the AIV improved by 5% for the modified AIV1 and 20% for the AIV2.

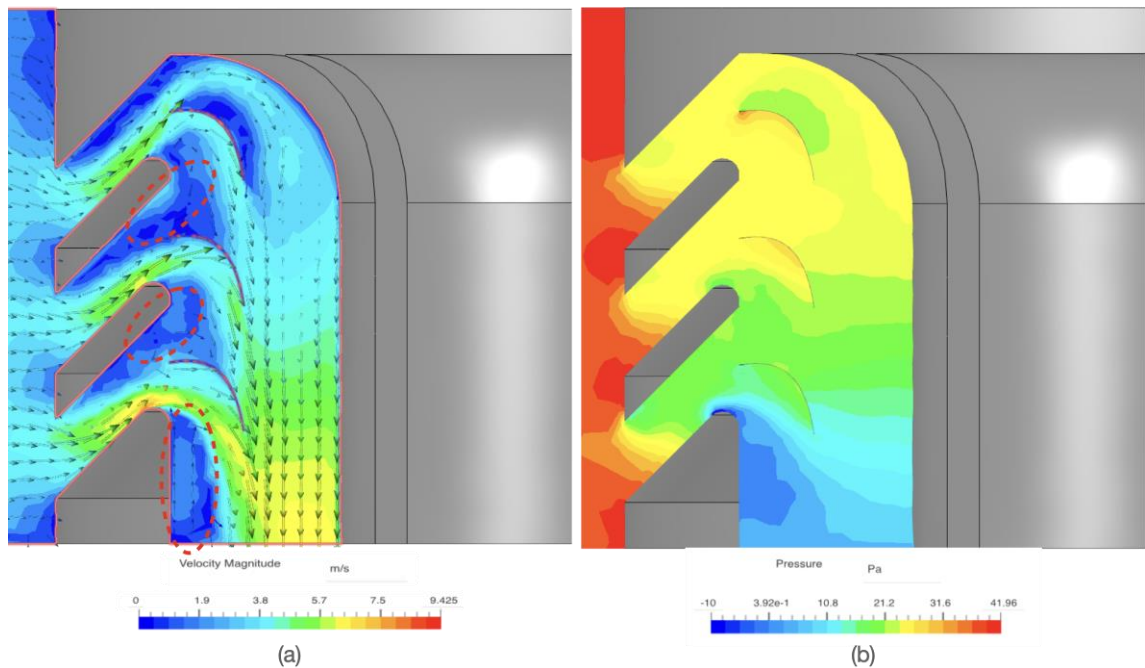


Figure 4.29. Contours of (a) velocity and (b) pressure of the modified AIV2 at velocity of 6 m/s.

To validate CFD simulation results from SimScale, a series of CFD simulations were executed for the modified AIV1 performance. The CFD simulation results of the

modified AIV1 using Autodesk CFD was visualised and presented. Figure 4.30 shows the contours of the velocity and pressure of the modified AIV1 at 6 m/s velocity. Figure 4.30a shows that the modified AIV1 induced airflow that streamed downward through the chamber. With the flow circulating inside the chamber, an average velocity of 0.34 m/s was recorded. Appendix Figure A2 and A3 illustrate the flow behaviour of the modified AIV1 within the chamber. Additionally, an average pressure of -10 Pa was registered inside the chamber (see Figure 4.30b). From this observation, The uniform negative pressure throughout the chamber indicates that the supply flow rate was insufficient to counterbalance the exhaust flow rate (Calautit et al., 2015). The modified AIV1 and modified 10B-TV did not correspond to the acknowledged underperformance of the modified AIV1 in terms of air supply, as shown in Figure 4.31. It is worth noting that the exhaust flow rate CFD result for the modified AIV1, obtained from Autodesk CFD, was 12% lower than the results from SimScale.

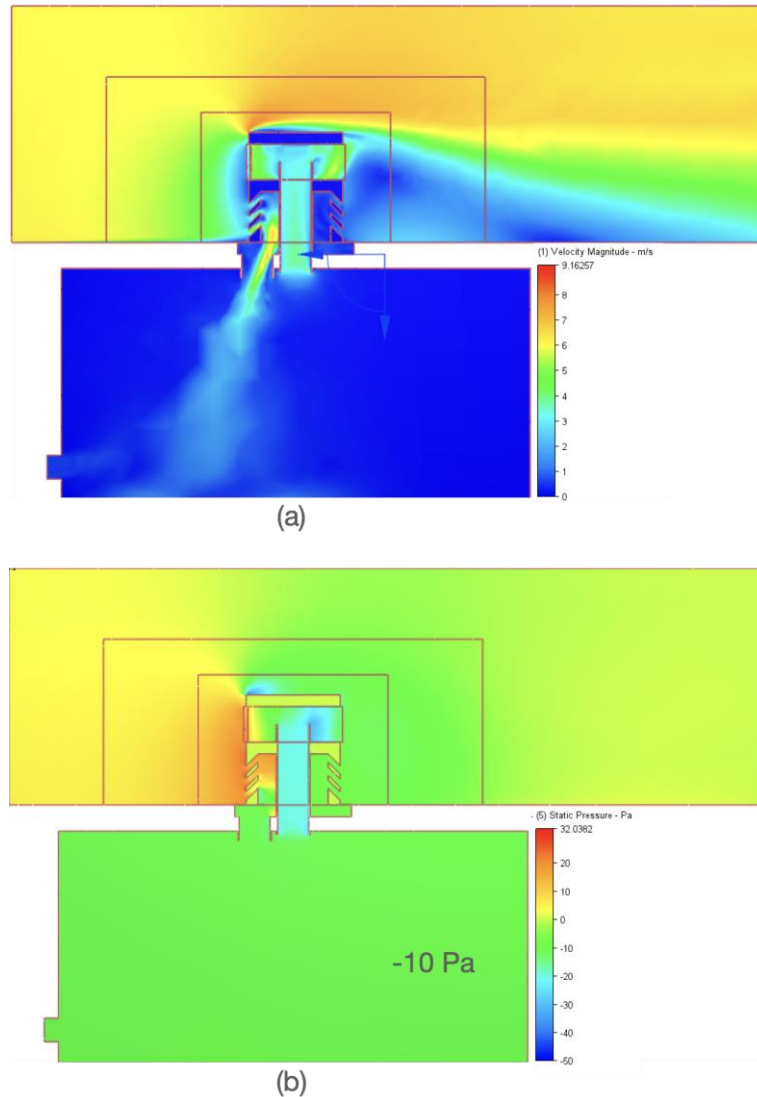


Figure 4.30. Cross-sectional plane of modified AIV1: (a) velocity contour and (b) pressure contour.

Several potential explanations for this discrepancy could be involved input data for CFD analysis settings or errors in extracting results. The most likely reason could be attributed to an error in the position of result extraction. Appendix Figure A4 illustrates the position of results extraction for each software. The numerical results in SimScale were extracted directly at the fitting between the supply channel and the duct leading to the chamber, while the result extracted from Autodesk occurred at



the duct leading to the chamber. In Autodesk CFD case, the flow losses were factored in as the airflow traversed through or within the duct, whereas flow losses were not taken into consideration for the SimScale case.

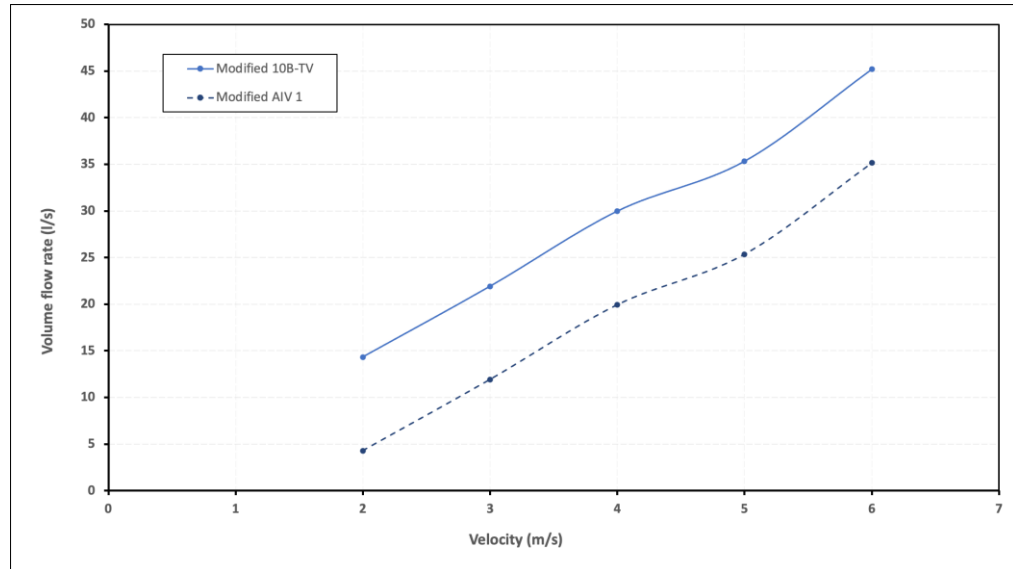


Figure 4.31. Comparison of ventilation performance of the modified AIV1 and the modified 10B-TV.

In conclusion, this chapter has demonstrated the potential for improving the performance of the AIV by implementing strategic modifications to its design features. The modified AIV1 and AIV2 models have exhibited increased airflow rates, reduced pressure drops, and minimised recirculation zones, as evidenced by the detailed analysis presented throughout this chapter. These promising results indicate that the adjustments made to the AIV designs have effectively contributed to enhancing the overall efficiency of the turbine ventilator system.

Moreover, the utilisation of the CFD simulations has proven to be a valuable tool in assessing and validating the performance of the modified AIV models. The CFD

simulations provided insightful data on the flow behaviour, pressure, and velocity within the turbine ventilator system, thereby enabling a comprehensive evaluation of the modifications implemented. It is important to acknowledge that while the modified AIV1 and AIV2 models have shown significant improvements, there is still room for further optimisation and refinement of their designs.

## 5. Conclusions

This study set out to investigate an innovative home ventilation system integrated with a wind-driven turbine ventilator, with the primary objectives reducing energy consumption and improving indoor air quality in residential buildings. The focal point of the research was the evaluation performance of the proposed turbine ventilator (see Figure 3.2) and its potential as an alternative solution for future home ventilation, both in new builds and conventional dwellings.

During the initial stages of the research, certain challenges arose concerning the limitations of the CFD software. Firstly, due to SimScale's capabilities, the proposed computational domain (Figure 3.6) could not be investigated as a whole; instead, it was divided into two separate parts for CFD simulations of air extraction and ventilation performance. Secondly, a desired turbulence model was unavailable in the employed CFD software. Lastly, limited computational resources posed additional challenges throughout the study.

CFD simulations were conducted using SimScale and Autodesk CFD software to predict the ventilation performance of the proposed turbine ventilator model. The CFD simulations initially explored the influence of blade profile by testing 2-blade (2B-TV) and 8-blade (8B-TV) models. The numerical results demonstrated that the 8B-TV outperformed the 2B-TV by 66% at velocity magnitudes of 3 m/s and above. The maximum exhaust flow rate induced by the 8B-TV reached 87.52 l/s at a wind speed of 6 m/s, surpassing the minimum ventilation rate. Although the 10B-TV was modified, it did not yield any improvement in ventilation performance.

An observation of the CFD results with experimental findings from other studies was conducted to validate the results. The present study's findings were found to be in concordance with the results of a 250 mm straight vane turbine ventilator by Khan et al. (2008b).

The initial design of the air intake vent (AIV) was tested, yielding a maximum air supply flow rate of 38.25 l/s at 6 m/s. However, this design did not meet the minimum ventilation rate, requiring modifications to enhance its ventilation performance. Consequently, the modified AIV1 and AIV2 designs resulted in a higher supply flow rate than the original AIV by 5% and 20% respectively. The AIV2 design met the minimum requirement for 5-bedroom dwelling.

Additionally, the study focused on a limited number of blade profiles and AIV designs. While the research provided valuable insights into the performance of different blade profiles and modifications, it is essential to recognize that other blade designs and AIV configurations might yield even better performance.

As a preliminary design, the proposed turbine ventilator demonstrates promising potential for integration into home ventilation systems. With further refinement, this novel ventilation concept could serve as a greener and more sustainable alternative for future and conventional residential buildings. Although powerless turbine ventilators effectively induce exhaust air flow rates in industrial settings, they are often considered unnecessary for domestic ventilation systems due to factors such as working environment requirements, visual pollution, and unreliable resource availability. In comparison to HVAC systems, which are perceived as more energy-

efficient and effective in providing adequate ventilation, turbine ventilators are often underrated. Developing a new ventilation system that incorporates a low-carbon turbine ventilator to maximise natural wind energy for ventilation and energy savings would present a more cost-effective and environmentally friendly solution for domestic dwellings.

### 5.1. Research Limitations

One significant research limitation was the constraint imposed by the CFD software. The study faced several challenges related to the software used, such as the inability to analyse the entire computational domain as a whole in SimScale. Instead, the domain had to be divided into separate parts for CFD simulations of air extraction and ventilation performance.

Another limitation was the unavailability of specific turbulence models in the CFD software, which could have further improved the reliability of the results. The study relied on the available models, which might not have been the most suitable for the specific problem being investigated.

Limited computational resources also posed a challenge throughout the study. The available resources might have restricted the complexity and refinement of the simulations, potentially affecting the overall accuracy and reliability of the results.

Lastly, the study relied on the comparison of CFD results with experimental findings from other studies for validation purposes. Although the findings were found to be in agreement with those of previous research, it is important to note that experimental

validation with physical models was not conducted as part of this study. Consequently, there might be discrepancies between the CFD predictions and real-world performance that have not been identified.

Despite these limitations, the study provides a valuable contribution to the understanding of the potential of wind-driven turbine ventilators in home ventilation systems. Future research should address these limitations and further explore other design options to optimize the performance of these systems.

## 6. Future works

The current study has provided significant insights into potential of an innovative home ventilation system that incorporates a wind-driven turbine ventilator. However, several areas remain unexplored, demanding further research. Based on the findings of the present study and relevant literature, the following future research directions are proposed:

- The present study has evaluated various configurations of the turbine ventilator and air intake vent, demonstrating improvements in ventilation performance. Future research should attempt to optimise the design of these components by conducting comprehensive parametric studies and drawing from existing literature on similar systems.
- Heat recovery was not addressed in this study. Given the objective of minimising energy consumption for space heating, further investigations should examine the potential for integrating a heat recovery unit with the proposed turbine ventilator. This research should emphasise the efficiency and practicality of incorporating heat recovery technologies in such systems.
- As wind is an intermittent energy source, additional energy sources may be necessary to maintain consistent operation of the ventilation system in the absence of wind. Future research should explore the integration of alternative energy sources, such as photovoltaic systems or energy storage solutions, to ensure reliable and continuous operation of the ventilation system.

- The present study employed a single turbulence model for the CFD analysis. To enhance the accuracy of predictions and ensure a closer representation of real-world conditions, future research should explore broader range of turbulence models, selecting those most suitable for the specific application of wind-driven turbine ventilators.
- Experimental validation of the CFD results via wind tunnel testing is crucial to assess the accuracy and reliability of the simulation models. Once the design has been optimised, future research should conduct a physical wind tunnel test in a laboratory setting and compare these results with the CFD predictions.
- Implementing control systems and sensors in the proposed ventilation system could enable efficient monitoring and control for indoor air quality, providing a more comfortable and healthy living environment. It recommends exploring the integration of smart controls and Internet of Thing technologies, which can enhance overall system performance, energy efficiency, and user experience.
- Conducting long-term performance assessments of the proposed turbine ventilator system in various climate conditions and geographical locations will prove valuable insights into the system's adaptability, reliability, and effectiveness in different settings.

Addressing these future research directions will contribute to the advancement of a more efficient, sustainable, and reliable home ventilation system that harnesses



wind energy and other renewable resources. This effort aligns with the broader goal of promoting environmentally friendly solutions in the built environment.

## Reference

- Abu-Zidan Y, Mendis P and Gunawardena T (2021) Optimising the computational domain size in CFD simulations of tall buildings. *Heliyon* 7(4): e06723.
- Adam N, Mohd ariffin Mka and Farahani A (2010) Simulation of Airflow and Aerodynamic Forces Acting on a Rotating Turbine Ventilator. *American Journal of Engineering and Applied Sciences* 3.
- Ahmad MI, Mansur FZ and Riffat S (2016) Applications of Air-to-Air Energy Recovery in Various Climatic Conditions: Towards Reducing Energy Consumption in Buildings. *Renewable Energy and Sustainable Technologies for Building and Environmental Applications*. pp.107-116.
- Akwa JV, Vielmo HA and Petry AP (2012) A review on the performance of Savonius wind turbines. *Renewable and Sustainable Energy Reviews* 16(5): 3054-3064.
- Alom N and Saha UK (2019) Influence of blade profiles on Savonius rotor performance: Numerical simulation and experimental validation. *Energy Conversion and Management* 186: 267-277.
- Alsailani M, Montazeri H and Rezaeiha A (2021) Towards optimal aerodynamic design of wind catchers: Impact of geometrical characteristics. *Renewable Energy* 168: 1344-1363.
- Anbarsooz M (2016) Aerodynamic performance of helical Savonius wind rotors with 30° and 45° twist angles: Experimental and numerical studies. *Proceedings of the Institution of Mechanical Engineers, Part A: Journal of Power and Energy* 230(6): 523-534.
- Autodesk CFD (2019) *User's Guide*. Available at: <https://help.autodesk.com/view/SCDSE/2019/ENU/?guid=GUID-94E433C2-1580-4575-A6FA-2E7F22A23EB6> (accessed 15th December).
- Baker C, Johnson T, Flynn D, et al. (2019) Chapter 4 - Computational techniques. In: Baker C, Johnson T, Flynn D, et al. (eds) *Train Aerodynamics*. Butterworth-Heinemann, pp.53-71.

- BEIS Df (2019) UK ENERGY IN BRIEF 2019. In: Department for Business EaS (ed). Department for Business, Energy and Industrial Strategy.
- Bradford Ventilation (2023) *Commercial & Industrial Ventilation*. Available at: <https://www.bradfordventilation.com.au/commercial-industrial-ventilation> (accessed 20th April).
- Calautit JK, Hughes BR and Shahzad SS (2015) CFD and wind tunnel study of the performance of a uni-directional wind catcher with heat transfer devices. *Renewable Energy* 83: 85-99.
- Calautit JK, O'Connor D, Tien PW, et al. (2020) Development of a natural ventilation windcatcher with passive heat recovery wheel for mild-cold climates: CFD and experimental analysis. *Renewable Energy* 160: 465-482.
- Change DoEaC (2010) 2050 Pathways Analysis. In: Change DoEaC (ed). Department of Energy and Climate Change.
- Chen T, Huang C and Kuo Y (2019) Numerical Study on Air Extraction Performance of Rooftop Ventilators. *Journal of Aeronautics, Astronautics and Aviation* 51: 075 - 086.
- Cho H, Cabrera D, Sardy S, et al. (2021) Evaluation of performance of energy efficient hybrid ventilation system and analysis of occupants' behavior to control windows. *Building and Environment* 188.
- CORDIS (2019) *Roof top wind turbine for urban areas*. Available at: <https://cordis.europa.eu/article/id/244881-wind-turbine-for-city-rooftops> (accessed 28 June).
- Delwati M, Merema B, Breesch H, et al. (2018) Impact of demand controlled ventilation on system performance and energy use. *Energy and Buildings* 174: 111-123.
- Dimitroulopoulou C (2012) Ventilation in European dwellings: A review. *Building and Environment* 47: 109-125.
- Dodoo A, Gustavsson L and Sathre R (2011) Primary energy implications of ventilation heat recovery in residential buildings. *Energy and Buildings* 43(7): 1566-1572.
- Drew DR, Barlow JF and Cockerill TT (2013) Estimating the potential yield of small wind turbines in urban areas: A case study for Greater London, UK. *Journal of Wind Engineering and Industrial Aerodynamics* 115: 104-111.
- Firth A, Zhang B and Yang A (2019) Quantification of global waste heat and its environmental effects. *Applied Energy* 235: 1314-1334.

- Franke J and Baklanov A (2007) *Best Practice Guideline for the CFD Simulation of Flows in the Urban Environment: COST Action 732 Quality Assurance and Improvement of Microscale Meteorological Models*.
- Ghanegaonkar PM, Jadhav GK and Garg S (2018) Performance improvement of turbo ventilators with internal blades. *Advances in Building Energy Research* 12(2): 164-177.
- Guillén-Lambea S, Rodríguez-Soria B and Marín JM (2016) Review of European ventilation strategies to meet the cooling and heating demands of nearly zero energy buildings (nZEB)/Passivhaus. Comparison with the USA. *Renewable and Sustainable Energy Reviews* 62: 561-574.
- Guyot G, Sherman MH and Walker IS (2018) Smart ventilation energy and indoor air quality performance in residential buildings: A review. *Energy and Buildings* 165: 416-430.
- Hammond GP and Stapleton AJ (2001) Exergy analysis of the United Kingdom energy system. *Proceedings of the Institution of Mechanical Engineers. Part A, Journal of power and energy* 215(2): 141-162.
- Hesaraki A, Myhren JA and Holmberg S (2015) Influence of different ventilation levels on indoor air quality and energy savings: A case study of a single-family house. *Sustainable Cities and Society* 19: 165-172.
- HM Government (2022) Approved Document F: Ventilation - Volume 1: Dwellings (2021 edition). In: Department for Levelling Up HaCaMoH, Communities & Local Government (ed). RIBA Publishing.
- Jadhav GK, Ghanegaonkar PM and Garg S (2016) Experimental and CFD analysis of turbo ventilator. *Journal of Building Engineering* 6: 196-202.
- Jason Palmer and Cooper I (2012) United Kingdom housing energy fact file. Reportno. Report Number|, Date. Place Published|: Institution|.
- Jomehzadeh F, Hussen HM, Calautit JK, et al. (2020) Natural ventilation by windcatcher (Badgir): A review on the impacts of geometry, microclimate and macroclimate. *Energy and Buildings* 226.
- Keirstead J, Jennings M and Sivakumar A (2012) A review of urban energy system models: Approaches, challenges and opportunities. *Renewable & sustainable energy reviews* 16(6): 3847-3866.
- Khan N, Su Y and Riffat SB (2008a) A review on wind driven ventilation techniques. *Energy and Buildings* 40(8): 1586-1604.
- Khan N, Su Y, Riffat SB, et al. (2008b) Performance testing and comparison of turbine ventilators. *Renewable Energy* 33(11): 2441-2447.

- Lai C-m (2003) Experiments on the ventilation efficiency of turbine ventilators used for building and factory ventilation. *Energy and Buildings* 35(9): 927-932.
- Lai C-M (2006) Prototype development of the rooftop turbine ventilator powered by hybrid wind and photovoltaic energy. *Energy and Buildings* 38(3): 174-180.
- Lai D, Qi Y, Liu J, et al. (2018) Ventilation behavior in residential buildings with mechanical ventilation systems across different climate zones in China. *Building and Environment* 143: 679-690.
- Lan X, Cao J, Lv G, et al. (2021) Simulation method for indoor airflow based on the Industry Foundation Classes model. *Journal of Building Engineering* 39.
- Lien S-TJ and Ahmed NA (2010) Numerical simulation of rooftop ventilator flow. *Building and Environment* 45(8): 1808-1815.
- Lien STJ and Ahmed NA (2011) Effect of inclined roof on the airflow associated with a wind driven turbine ventilator. *Energy and Buildings* 43(2-3): 358-365.
- Lin YP, Shieh TH, Chiang CM, et al. (2010) How the Rooftop Turbine Ventilator Powered by Hybrid Renewable Energy Affects Factory Ventilation Performance. *Proceedings of the Institution of Mechanical Engineers, Part E: Journal of Process Mechanical Engineering* 224(4): 275-279.
- Monodraught (2020) *Natural ventilation product brochure*. Available at: <https://www.monodraught.com> (accessed 2 June).
- Noman AA, Tasneem Z, Sahed MF, et al. (2022) Towards next generation Savonius wind turbine: Artificial intelligence in blade design trends and framework. *Renewable and Sustainable Energy Reviews* 168: 112531.
- Palmer J, Terry N and Kane T (2012) Early Findings: Demand side management. In: Change DoEC (ed). Department of Energy & Climate Change.
- Patankar SV (1980) *Numerical heat transfer and fluid flow*. London: McGraw-Hill.
- Pérez-Lombard L, Ortiz J and Pout C (2008) A review on buildings energy consumption information. *Energy and Buildings* 40(3): 394-398.
- Peter G. Taylor, Olivier Lavagne d'Ortigue, Michel Francoeur, et al. (2010) Final energy use in IEA countries: The role of energy efficiency. *Energy Policy* 38(11): 6463-6474.
- Rhodes N (1995) Heating, ventilating and air conditioning analysis and design. *Proceedings of the Institution of Mechanical Engineers* 209(2): 163.

- Rimdžius D, Bielskus J, Martinaitis V, et al. (2018) Experimental Evaluation of Turbine Ventilators Performance under Different Test Conditions. *E3S Web of Conferences* 64.
- Russell M, Sherman M and Rudd A (2007) Review of Residential Ventilation Technologies. *HVAC&R Research* 13(2): 325-348.
- Saadatian O, Haw LC, Sopian K, et al. (2012) Review of windcatcher technologies. *Renewable and Sustainable Energy Reviews* 16(3): 1477-1495.
- Santos HRR and Leal VMS (2012) Energy vs. ventilation rate in buildings: A comprehensive scenario-based assessment in the European context. *Energy and Buildings* 54: 111-121.
- Shieh T-h, Chang P-C, Chiang C-m, et al. (2010) Potential assessment of an innovative hybrid ventilator for building ventilation. *Journal of Mechanical Science and Technology* 24(11): 2341-2345.
- Shun S and Ahmed NA (2008) Utilizing wind and solar energy as power sources for a hybrid building ventilation device. *Renewable Energy* 33(6): 1392-1397.
- SIMSCALE (2020) *SimScale Documentation*. Available at: <https://www.simscale.com/docs/> (accessed 11 June).
- Streckienė G, Motuzienė V, Rimdžius D, et al. (2018) Simulation of Annual Functionality of Roof Turbine Ventilator. *E3S Web of Conferences* 64.
- Tahani M, Rabbani A, Kasaeian A, et al. (2017) Design and numerical investigation of Savonius wind turbine with discharge flow directing capability. *Energy* 130: 327-338.
- Tan YC, Ismail M and Ahmad MI (2016) Turbine Ventilator as Low Carbon Technology. *Renewable Energy and Sustainable Technologies for Building and Environmental Applications*. pp.167-174.
- Tian W, Mao Z and Ding H (2019) Numerical study of a passive-pitch shield for the efficiency improvement of vertical axis wind turbines. *Energy Conversion and Management* 183: 732-745.
- Turner WJN and Awbi HB (2014) Experimental investigation into the thermal performance of a residential hybrid ventilation system. *Applied Thermal Engineering*. DOI: 10.1016/j.applthermaleng.2014.12.026.
- Ventilationland (2021) *Anjo Wind-powered fans*. Available at: <https://www.ventilationland.co.uk/product/18188/wind-powered-fan-vt-turbine-150mm-stainless-steel-440m3-h.html> (accessed 28 June).
- WHO (2021) *Roadmap to improve and ensure good indoor ventilation*

in the context of COVID-19. Available at: <https://www.who.int/publications/i/item/9789240021280> (accessed 25 June).

Zemitis J and Borodinecs A (2019) Energy saving potential of ventilation systems with exhaust air heat recovery. *IOP Conference Series: Materials Science and Engineering* 660: 012019.

Zhai Z, Johnson M-H and Krarti M (2011) Assessment of natural and hybrid ventilation models in whole-building energy simulations. *Energy and Buildings* 43(9): 2251-2261.

Zhou T and Rempfer D (2013) Numerical study of detailed flow field and performance of Savonius wind turbines. *Renewable Energy* 51: 373-381.

Zhou Y and Stathopoulos T (1997) A new technique for the numerical simulation of wind flow around buildings. *Journal of Wind Engineering and Industrial Aerodynamics* 72(1-3): 137-147.

## Appendix Tables

Table A1. Minimum ventilation rate (air extraction)

Ventilation rates for air extraction		
Room type	Continuous extract	
	high rate (l/s)	low rate (l/s)
Kitchen	13	
Utility room	8	Should be at least supply air flow rates in Table 1
Bathroom	8	
Sanitary accommodation	6	

Table A2. Minimum ventilation rate (fresh air supply)

Whole dwelling ventilation rates for air supply	
No. of bedrooms in dwelling	Ventilation rates (l/s)
	1
2	25
3	31
4	37
5	43

Table A3. Ventilation rate of the air intake vent

AIV					
Velocity	Supply flow rates		Pressure at supply channel		
m/s	m <sup>3</sup> /s	l/s	Min. Pa	Aver. Pa	Max. Pa
1	0.0053	5.3	-0.019	0.55	0.95
2	0.0116	11.6	-0.073	2.59	4.37
3	0.0157	15.7	-0.114	4.83	8.23
4	0.0212	21.2	-0.182	8.75	15.31
5	0.0266	26.6	-0.2821	13.89	24.19
6	0.0383	38.25	-0.5247	27.26	44.39

Table A4. SimScale' supply flow rate of modified AIV1

Modified AIV 1			
Velocity	Supply flow rate		Static Pressure
(m/s)	(m <sup>3</sup> /s)	(l/s)	(Pa)
6	0.0404	40.38	19.7

Table A5. SimScale' supply flow rate of modified AIV2

Modified AIV 2			
Velocity	Supply flow rate		Static Pressure
(m/s)	(m <sup>3</sup> /s)	(l/s)	(Pa)
6	0.0481	48.11	17.86



Table A6. Autodesk's exhaust flow rate of modified 10B-TV

Modified 10B-TV				
Velocity	Rotational speed	Exhaust flow rate		Static Pressure
(m/s)	(RPM)	(m <sup>3</sup> /s)	(l/s)	(Pa)
2	48	0.0143	14.33	-1.13
3	60	0.0127	21.91	-3.75
4	115	0.0093	29.97	-8.23
5	167	0.0079	35.32	-12.28
6	216	0.0061	45.18	-20.21

Table A7. Autodesk's supply flow rate of modified AIV1

Modified AIV 1			
Velocity	Supply flow rate		Static Pressure
(m/s)	(m <sup>3</sup> /s)	(l/s)	(Pa)
2	0.0043	4.28	0.43
3	0.0119	11.92	1.73
4	0.0199	19.94	4.27
5	0.0254	25.36	7.78
6	0.0352	35.16	11.83

# Appendix Figures

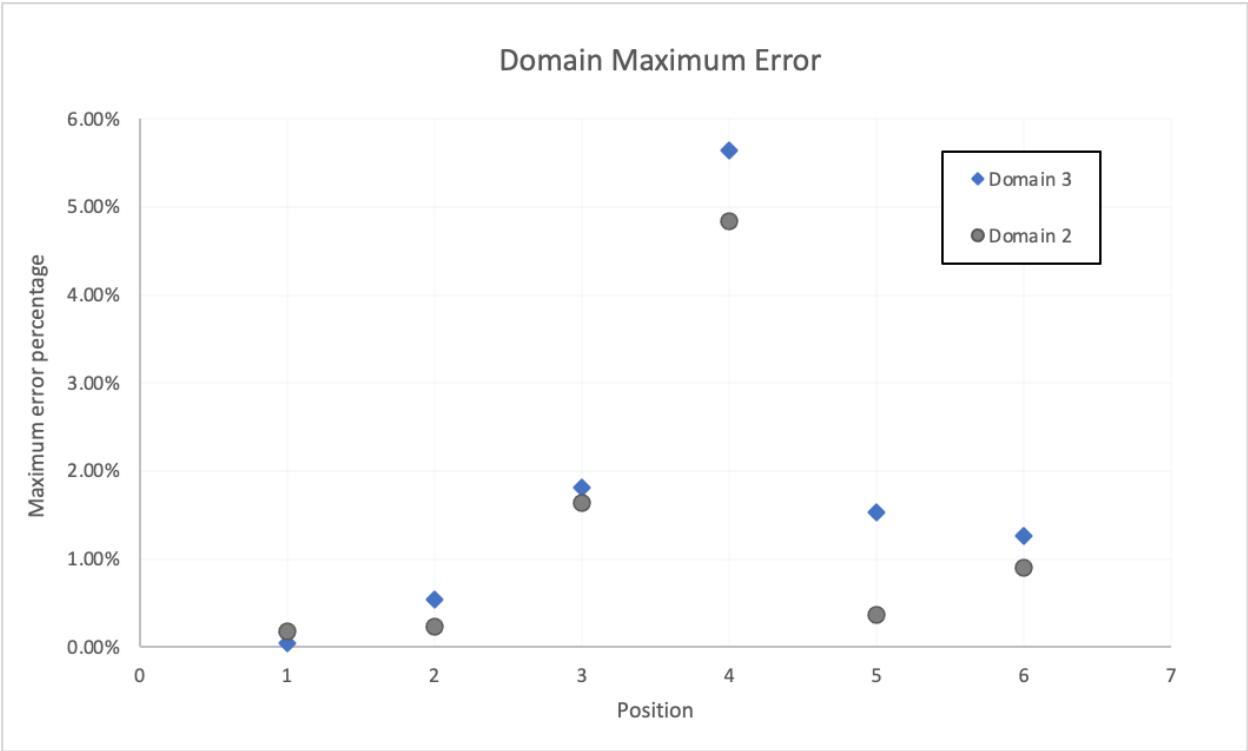


Figure A1. Domain maximum error percentage.

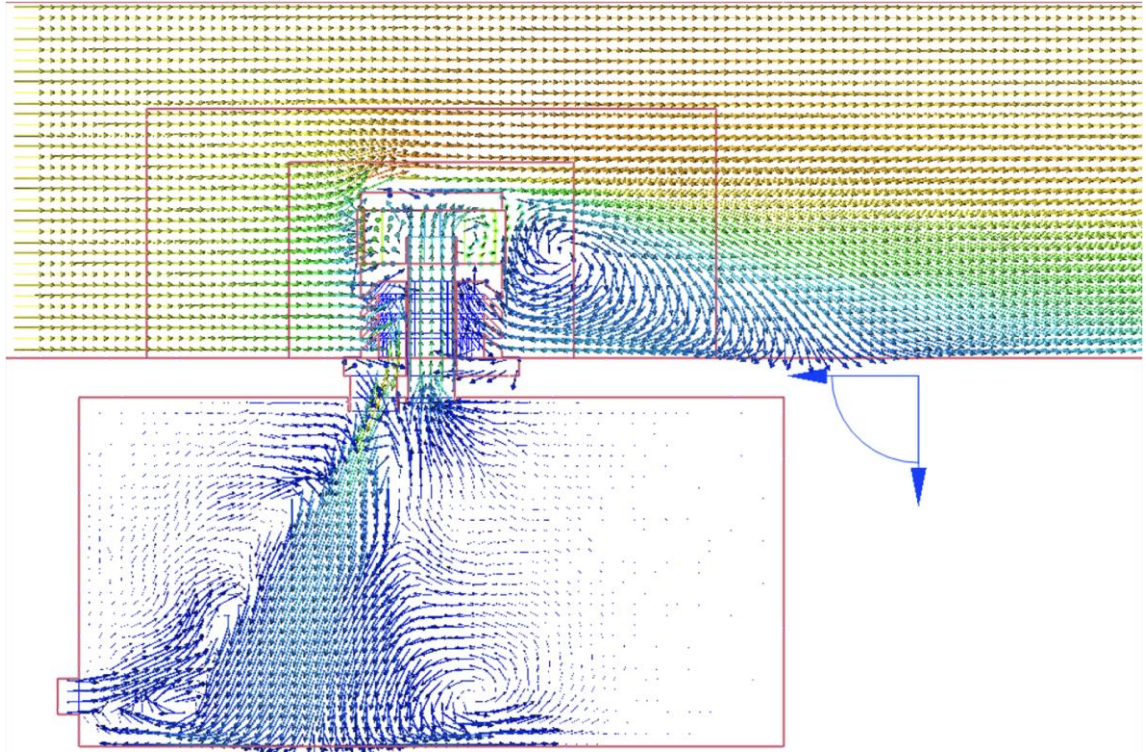


Figure A2. Velocity vector of the modified AIV1 for visualizing flow behaviour in the chamber.

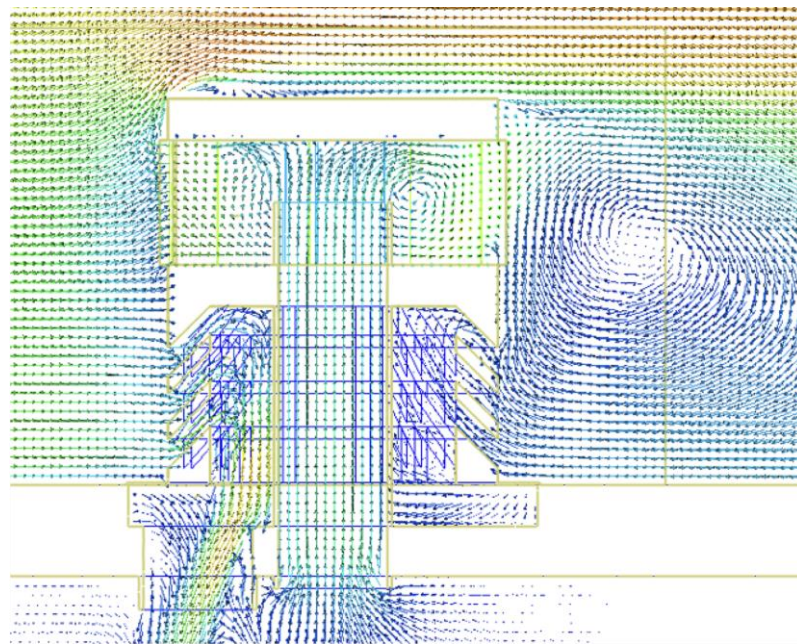


Figure A3. Velocity vector of the modified AIV1 for visualizing flow behaviour within the mode.

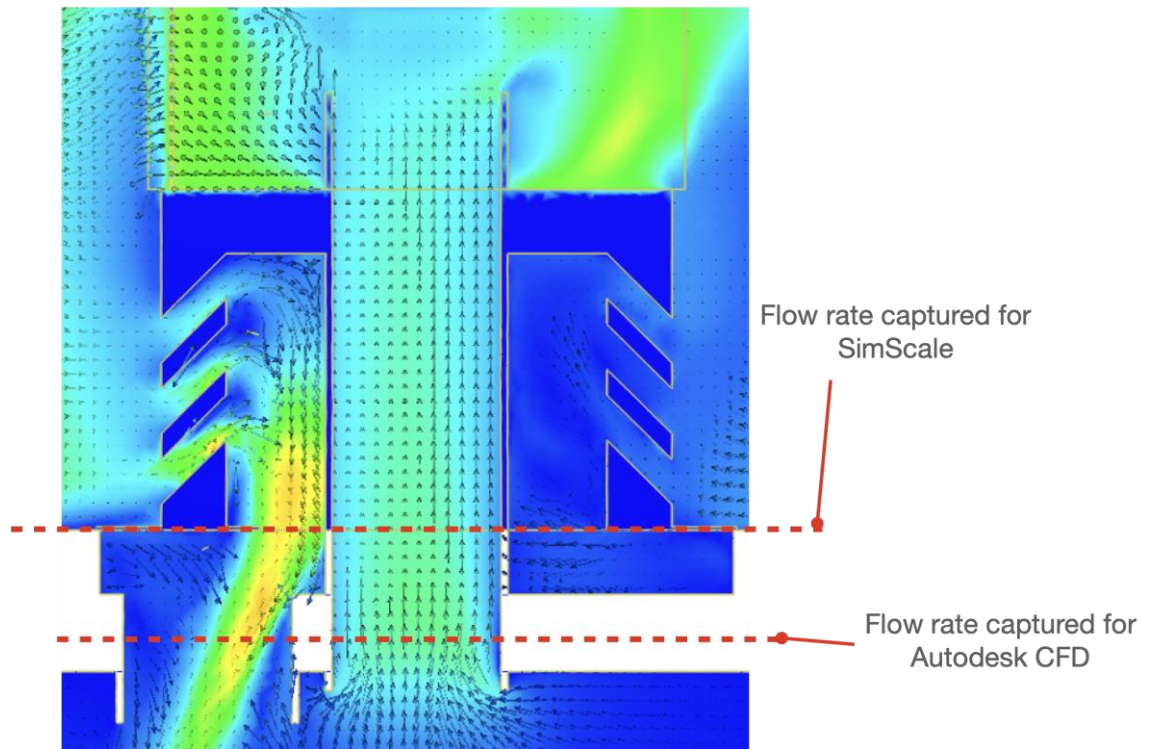


Figure A4: The position of result extraction for the air supply rate.